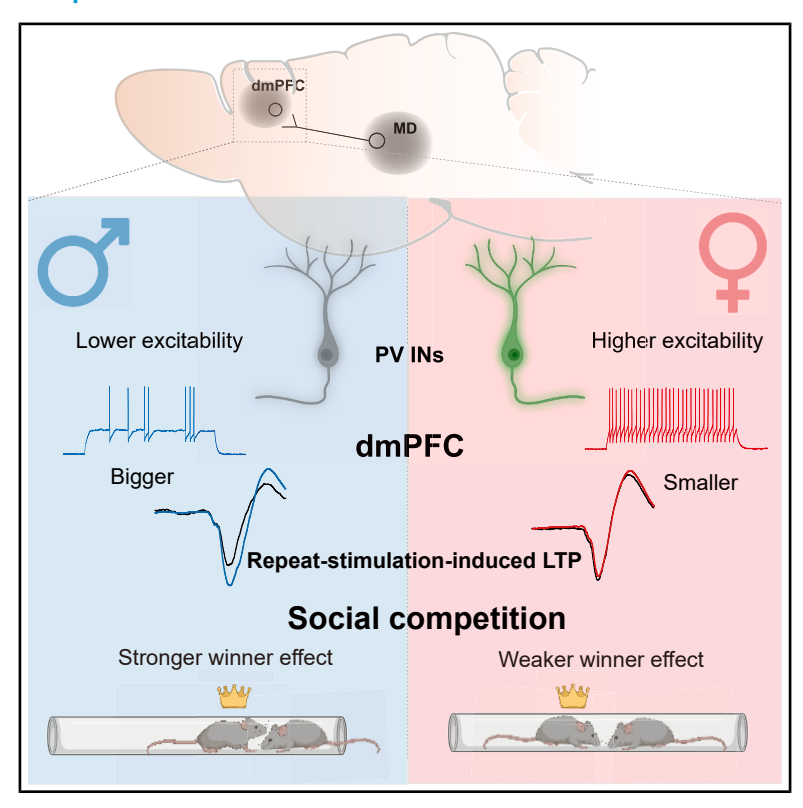
Neuron

Neural mechanism of the sexually dimorphic winner effect in mice

Graphical abstract



Authors

Diyang Zheng (郑迪旸), Qiuhong Xin (辛秋红), Shuimu Jin (金水木), Anqi Zhou (周安琪), Xiaoning Jia (贾晓宁), Yi Tan (檀毅), Hailan Hu (胡海岚)

Correspondence

huhailan@zju.edu.cn

In brief

Zheng et al. find that female mice establish social hierarchies but exhibit a weaker winner effect compared with males. This difference is linked to attenuated LTP at MDT-to-dmPFC synapses due to heightened excitability of dmPFC parvalbumin interneurons. These findings reveal the circuit and neuronal mechanisms underlying sexually dimorphic dominance behaviors.

Highlights

- Females form hierarchies, with the dmPFC bidirectionally regulating dominance behaviors
- Females take longer to form hierarchies and show a weaker winner effect than males
- Females show reduced LTP at MDT-dmPFC synapses and increased PV-IN excitability
- Bidirectional dmPFC PV-IN modulation regulates LTP/winner effect in a sex-dimorphic manner



Neuron



Article

Neural mechanism of the sexually dimorphic winner effect in mice

Diyang Zheng (郑迪旸),^{1,2} Qiuhong Xin (辛秋红),^{1,2} Shuimu Jin (金水木),^{1,2} Anqi Zhou (周安琪),^{1,2} Xiaoning Jia (贾晓宁),^{1,2} Yi Tan (檀毅),² and Hailan Hu (胡海岚)^{1,2,3,4,5,*}

¹Department of Neurobiology, Affiliated Mental Health Center & Hangzhou Seventh People's Hospital and School of Brain Science and Brain Medicine, Zhejiang University School of Medicine, Hangzhou 310058, China

²Liangzhu Laboratory, MOE Frontier Science Center for Brain Science and Brain-Machine Integration, State Key Laboratory of Brain-Machine Intelligence, New Cornerstone Science Laboratory, Zhejiang University, Hangzhou 311121, China

³Nanhu Brain-Computer Interface Institute, Zhejiang University, Hangzhou 311121, China

⁴Institute of Fundamental and Transdisciplinary Research, Zhejiang University, Hangzhou 311121, China

⁵Lead contact

*Correspondence: huhailan@zju.edu.cn https://doi.org/10.1016/j.neuron.2025.09.029

SUMMARY

The "winner effect," where prior victories increase the likelihood of future wins, profoundly shapes social hierarchy dynamics and competitive motivation. Although human literature suggests a less pronounced winner effect in females, the neural mechanisms underlying these sex differences remain unclear. Here, we show that, compared with male mice, female mice take longer to form social hierarchies and exhibit a weaker winner effect. The dorsomedial prefrontal cortex (dmPFC), crucial for social dominance in males, plays a similar role in female mice. However, female mice exhibit reduced long-term potentiation (LTP) at the mediodorsal thalamus (MDT)-to-dmPFC synapses. *In vitro* recordings revealed that female mice have heightened excitability of dmPFC parvalbumin interneurons (PV-INs). Modulation of dmPFC PV-IN activity regulates LTP and the winner effect in a sexually dimorphic manner. This work identifies dmPFC PV-INs as a target for enhancing the winner effect, establishing a circuit-level framework for sex differences in competitive behaviors.

INTRODUCTION

The "winner effect," a phenomenon in which prior success in competition increases the probability of future victories, is a key driver of social hierarchy dynamics, reinforcing dominance and stabilizing competitive relationships within groups. ^{1–5} At the individual level, the winner effect enhances competitive motivation, builds self-confidence, and fosters resilience, ^{6–8} enabling individuals to thrive in challenging environments. Although the winner effect has been extensively studied in males, its expression in females and the neural mechanisms underlying potential sex differences remain poorly understood compared with other innate behaviors. ^{9–11}

In males, the winner effect is closely tied to the dynamics of social hierarchy formation. Repeated competitive successes strengthen dominance behaviors, creating positive feedback loops that stabilize hierarchical structures. 12–15 Neural studies in male mice have identified the dorsomedial prefrontal cortex (dmPFC) as a key brain region mediating these effects. 16–19 Specifically, repeated winning experiences enhance synaptic plasticity at the mediodorsal thalamus (MDT)-to-dmPFC pathway through long-term potentiation (LTP), a process that underlies

the reinforcement of dominance behaviors. These findings highlight the importance of the dmPFC in encoding and maintaining social hierarchies through the winner effect in male mice. However, whether similar mechanisms operate in females, and how sex differences in hierarchy formation arise, remain open questions. Unlike males, female mice show limited overt aggression in daily interactions, 10,20,21 raising the question of whether and how females establish dominance hierarchies despite this difference. Furthermore, the neural mechanisms mediating dominance behaviors in females remain largely unexplored, leaving a significant gap in our understanding of sex-specific regulation of social competition.

Emerging evidence suggests that the winner effect is less pronounced in females. In humans, men consistently exhibit a winner effect in competitive contexts such as tennis, judo, and video games, whereas women do not show the same pattern. 7.22-24 Similarly, in mice, repeated competitive experiences enhance aggression and dominance in males 6,8,25 but not in females. 26,27 Although males are strongly influenced by prior social experiences, females rely more on intrinsic attributes. 28 Male mice also exhibit stronger competitive feedback loops and earlier behavioral individualization, while females





show weaker competition effects and delayed behavioral differentiation. These findings suggest that sex differences in the winner effect may be phylogenetically conserved, with females relying less on prior winning experiences to establish their social ranks. However, the neural mechanisms driving these differences remain largely unexplored.

Here, we investigate the interplay between the winner effect and social hierarchy formation in male and female mice. Using behavioral paradigms such as the dominance tube test and the warm spot competition, we demonstrate that female mice can form social hierarchies but exhibit a weaker winner effect compared with males. We identify the dmPFC as a critical regulator of dominance behaviors in both sexes but reveal sex-specific differences in synaptic plasticity and neural circuitry. Specifically, female mice show reduced LTP at MDT-to-dmPFC synapses and heightened excitability of dmPFC parvalbumin interneurons (PV-INs). Modulation of PV-IN activity further demonstrates that these neurons regulate LTP and the winner effect in a sexually dimorphic manner. These findings provide new insights into the neural and circuit mechanisms underlying sex differences in the winner effect and its role in shaping social hierarchies.

RESULTS

Social hierarchy in female mice

We subjected female C57BL/6J mice to two types of dominance assays that had been previously established in male mice: the dominance tube test and the warm spot competition test (Figure 1).8,17 Female mice were group-housed, four per cage, for at least 1 week before being tested pairwise against their cagemates in the tube test and were ranked based on total winning times (Figure 1A). Similar to males (Figures S1A-S1G), female mice also showed highly transitive tube test ranks: in 160 out of 164 contests from 41 cages, ranks among any three cagemates were transitive, meaning that when mouse A wins against B and B wins against C. then A will win against C (Figure 1B). Consistent with this high transitivity, 90.2% (37 out of 41) of mouse cages formed a linear social diagram (Figure 1C). Following daily tube tests, ranks became more stable and more mice maintained the same rank status as the previous day (Figures 1D and 1E). The duration of contests from all rank pairs decreased significantly over time (Figure 1F), consistent with the phenomenon that intra-group competitions drop as social hierarchies stabilize.30 Moreover, the duration of the tube test was significantly shorter when the lowest-ranked mouse (rank 4) was involved or as rank distance increased (Friedman test with Dunn's multiple comparisons test; Figure 1G).

To further confirm that tube test ranks reflect dominance relationship in female mice, we conducted an additional assay, the warm spot test, 8 which involved different sensorimotor skills. In this test, four female cagemates competed for a warm, heated corner in a box with an ice-cold floor (Figure 1H). Dominant mice had a higher chance of pushing subordinate mice out of the warm spot, consequently spending more time in the warm spot. The cumulative time each female mouse spent in the warm spot correlated with its tube test rank (p = 0.014 for occupation time, p = 0.009 for rank, Pearson's correlation test; Figures 1I–1K; see STAR Methods). This cross-validation of

two dominance assays demonstrates that female mice can have dominant social interactions despite not being overtly aggressive.

dmPFC activity bidirectionally controls social hierarchy in female mice

Because the dmPFC has been strongly implicated in regulating social hierarchy behaviors in male mice, 8,17-19 we next tested whether it also played a critical role in female mice (Figure 2). To activate the dmPFC, we stereotactically injected an adeno-associated virus (AAV) expressing light-sensitive channelrhodopsin (ChR2)31 under the ubiquitously expressed CAG promoter (AAV2/9-CAG-ChR2) into the right dmPFC and implanted a fiber-optic cannula directly above the injection site (Figure 2A). After 4 weeks of viral expression, female mice were tested daily to obtain a stable rank (with no rank change for at least 4 continuous days). We then delivered blue light (473 nm) using a 100-Hz phasic protocol (9 ms per pulse, 4 pulses/s)8 to one of the female mice to activate its dmPFC immediately before it entered the tube to confront its opponent (see STAR Methods) (Figures 2B and 2C). Although photostimulation did not alter the rank status of control mice injected with AAV2/9-CAG-tdTomato (Figure 2E), it instantaneously induced winning in ChR2-expressing mice against previously dominant opponents (day 0, p = 0.027, two-way repeated measure ANOVA; Bonferroni multiple comparisons, Figures 2D, 2E, S2A, and S2B). Detailed video analysis revealed that, under photostimulation, the originally subordinate mice significantly increased effortful behaviors, including push and resistance, and decreased retreats (Figure 2F). Such photostimulation did not affect motor performance or anxiety level (Figures S3A-S3E).

We next examined whether dmPFC inhibition can quickly suppress dominance in female mice in the tube test. AAV expressing an enhanced variant of the light-sensitive inhibitory halorhodopsin (eNpHR3.0)³² under the ubiquitously expressed human synapsin promoter (AAV2/9-hSyn-eNpHR3.0) was bilaterally injected into the dmPFC (Figure 2G). Whole-cell recordings from acutely isolated dmPFC brain slices confirmed that 589-nm yellow light suppressed the eNpHR3.0-expressing dmPFC neurons, causing a significantly decreased spike number under current step injections (before versus lighting, p < 0.0001; lighting versus after, p = 0.014; Friedman test with Dunn's multiple comparisons test; Figure 2H). We then delivered constant yellow light to one female mouse from the four-mouse groups with stable ranks to inhibit its dmPFC during the entire tube test (Figure 2I). This induced, in seven out of eleven female mice, an immediate decline in rank (day 0, p = 0.008, two-way repeated measure ANOVA; Bonferroni multiple comparisons, Figures 2J, 2K, S2C, and S2D). Video analysis revealed that these lower-ranked female mice showed significantly decreased effortful behaviors, including push and resistance, and increased retreats (Figure 2L). Such photostimulation did not affect the ranks of control mice injected with AAV2/9hSyn-mCherry virus in the dmPFC (Figure 2K). Neither did it affect their motor performance or anxiety levels (Figures S3F-S3J).

Weaker winner effect in female mice

Despite the overall similarity in tube test performance between male and female mice, we did observe several differences. First, it took longer for female mice to establish a stable hierarchy



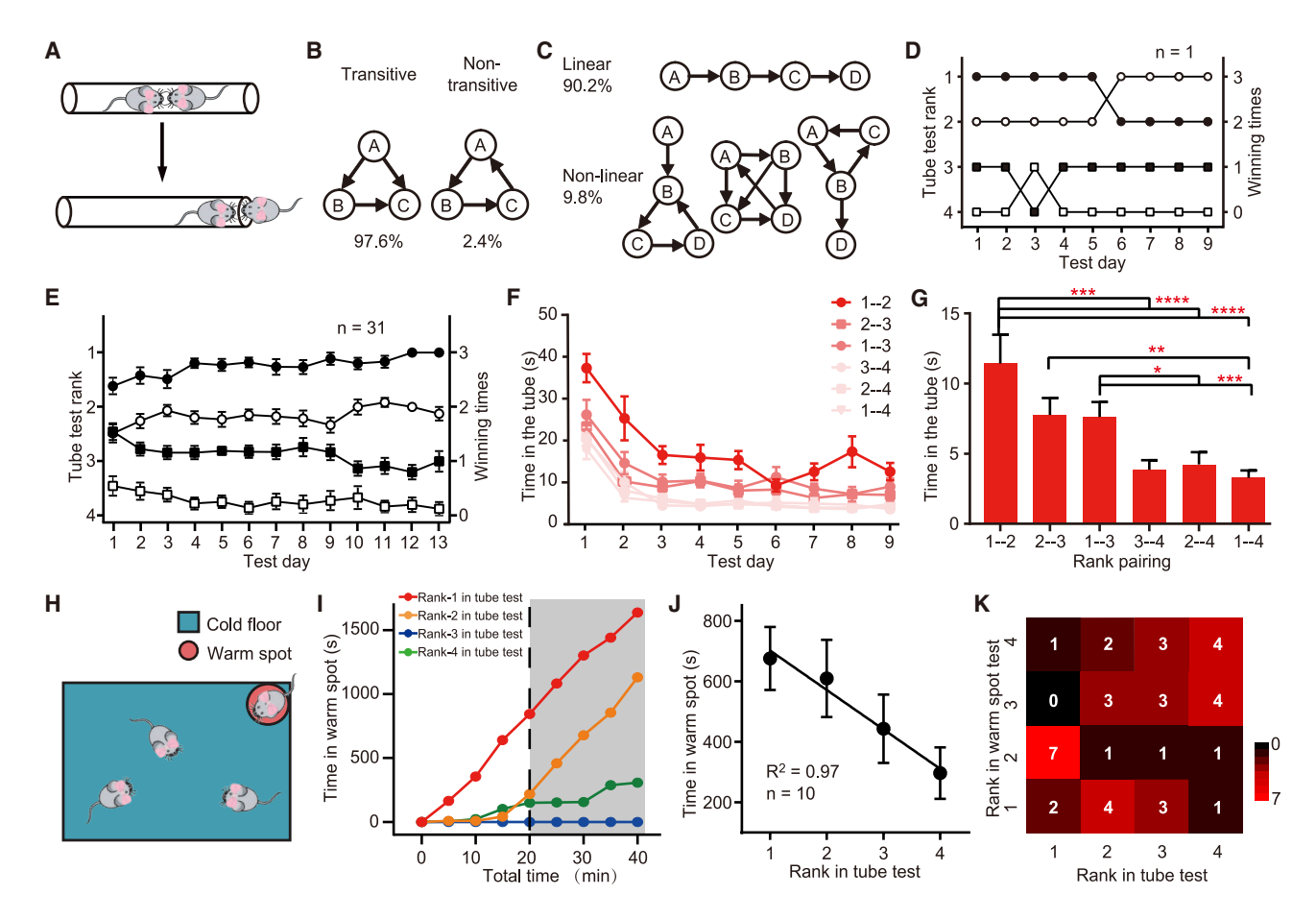


Figure 1. Social hierarchy in female mice

- (A) Schematic of tube test for female mice.
- (B) Illustration of a transitive and a nontransitive relation (n = 164 cases) in female mice.
- (C) Illustration of a linear and three nonlinear social diagrams for a cage of four female mice (n = 41 cages). 90.2% of cages formed a linear social diagram.
- (D) Example of rank positions in one cage of female mice tested daily over 9 days.
- (E) Summary graph for the 31 cages measured. Average rank positions of animals belonging to each rank group from the first test day.
- (F) Average time spent in the tube during encounters for each pairing condition across 9 test days (n = 22 cages), e.g., 1-2 stands for rank 1 against rank 2.
- (G) Time spent in the tube test for the six pairing conditions (n = 22 cages) on the first day of rank stabilization. Friedman test with Dunn's multiple comparisons test.
- (H) Schematic of the warm spot test. Four female mice compete for a heated warm corner (in red) in a cage with an ice-cold floor (in blue).
- (I) Cumulative time spent in the warm spot by four cagemates of different tube test ranks. The shaded area indicates the 20-min time window (20–40 min) used for rank-related quantification.
- (J) Correlation between time spent in the warm spot and social rank in the tube test. Pearson's correlation test, $\rho = 0.014$.
- (K) Contingency table showing the correlation between rank in the tube test and rank in the warm spot test. Number of animals in each category is shown, with color intensity indicating counts according to the scale on the right. Pearson's correlation test, $\rho = 0.009$.

Error bars indicate \pm SEM. *p < 0.05; **p < 0.01; ****p < 0.001; ****p < 0.0001.

See also Figure S1 and Table S1.

(Figures 3A–3C). When we quantified the percentage of mice maintaining the same rank as the previous day (defined as stability percentage), female mice showed lower stability (p = 0.03, two-way repeated measure ANOVA; Figure 3B) and took more trials than male mice to reach a stable hierarchy (p = 0.0033, Mann-Whitney test; Figure 3C). Second, female mice showed a weaker winner effect induced by repeated optogenetic stimulation of winning (Figures 3D–3F). Previously, we found that after 6 repeated wins induced by optogenetic stimulation of the dmPFC, all male mice maintained their new rank positions the

following day, reflecting the winner effect.⁸ To avoid the ceiling effect, we reduced the number of wins to 4–5 and found that, on the following day, although 78% of male mice maintained the new rank, only 22% of female mice held on to the new status (p = 0.018, Z test; Figures 3F and S4A). In addition to photostimulated winning, we also tried a behavior-based winning protocol: after determining the dominance relationship between a pair of mice, we induced repeated "forced wins" (4 times) in the subordinate mice by blocking their side of the tube using a dynamometer (Figure 3G). The forces applied to subordinate mice during



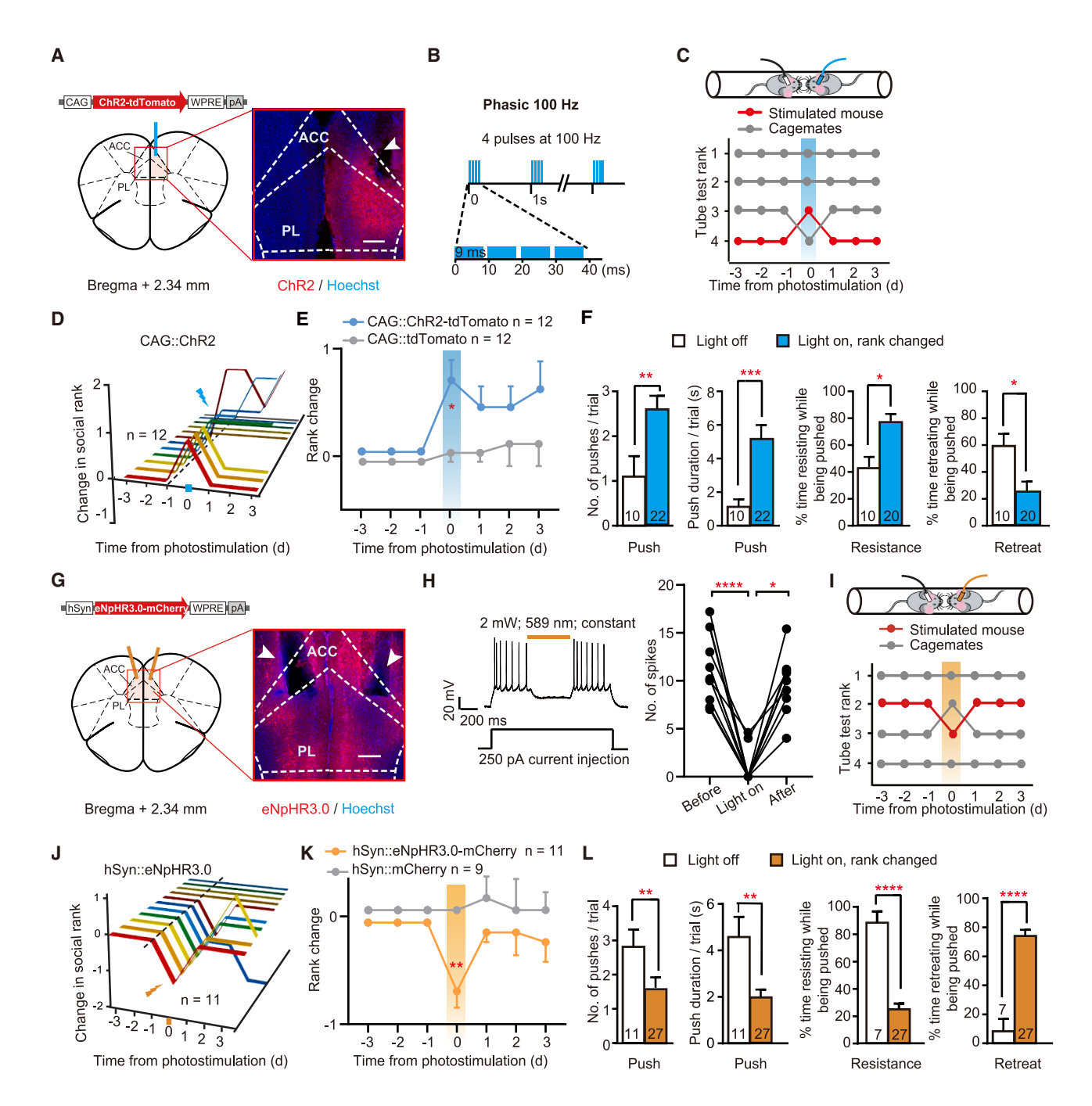


Figure 2. dmPFC activity bidirectionally controls social hierarchy in female mice

(A and G) Schematic illustrating the CAG::ChR2 (A) or the hSyn::eNpHR3.0 (G) viral construct, viral injection site, and optic fiber placement (indicated by white arrowhead) in the dmPFC, including the prelimbic cortex (PL) and part of the anterior cingulate cortex (ACC). Scale bar, 200 μ m.

(B) Schematic illustrating a 100-Hz phasic protocol of blue light photostimulation (473 nm, 9 ms per pulse, 4 pulses/s).

(C and I) Daily tube test results for a cage of female mice injected with CAG::ChR2 (C) or hSyn::eNpHR3.0 (I) virus, before and after acute dmPFC photostimulation of the rank 4 (C) or rank 2 (I) mouse on day 0.

(D and J) Summary of dmPFC photostimulation-induced rank change in mice injected with CAG::ChR2 (D) or hSyn::eNpHR3.0 (J) virus. Each line represents one animal.

(E and K) Average rank change in tube test under photoactivation (E) or photoinhibition (K) in the experimental and control groups. Light stimulation is delivered throughout the tube test on day 0. Two-way repeated measure ANOVA with Bonferroni multiple comparisons post hoc tests.

(F and L) Comparison of behavioral performance of the same CAG::ChR2 (F) or hSyn::eNpHR3.0 (L) mice during light-off and light-on trials. The number of trials is indicated in each bar. Only mice showing rank changes were analyzed. Mann-Whitney test.



their retreats, as measured by the dynamometer, gradually decreased, indicating the emergence of the winner effect (Figure 3H). On the next day, again, significantly more male mice maintained the new dominance position than did the female mice (91% in males versus 43% in females, p = 0.013, Z test; Figure 3I).

As the opponent mice in the above two paradigms also experienced repeated losing, the end results may reflect both the winner effect of the manipulated mice and the loser effect of the opponent mice. In order to distinguish whether female mice differ from male mice in the winner or the loser effect, we next tried a third paradigm in which different opponent mice were used during the repeated winning trials and the final test (Figures 3J and 3K). Specifically, to isolate the winner effect, mice were tested against a different opponent after three natural wins against a weaker opponent (see STAR Methods). 33,34 Under this scenario, male mice defeated their naive opponents at a high success rate, whereas female mice performed at chance levels (p = 0.001 for male, p = 0.79 for female, binomial test; Figure 3J). To isolate the loser effect, mice were tested against a different opponent after three natural losses to a stronger opponent.33,34 Both male and female mice lost to their naive opponents at high rates (p = 0.0001 for male, p = 0.0034for female, binomial test; Figure 3K). Taken together, compared with male mice, female mice showed a similar loser effect (p = 0.89, Z test; Figure 3K) but a lesser winner effect (p = 0.023, Z test; Figure 3J). We also investigated the effect of estrous cycle and found that it did not impact the winner effect in female mice (p = 0.94, Z test; Figures S4B and S4C).

Reduced LTP in the MDT-dmPFC circuit of female mice

The neural underpinning of the winner effect in male mice has been previously attributed to LTP in the MDT-dmPFC circuit.8 Therefore, in order to explore the neural mechanisms underlying sexual dimorphism in the winner effect, we employed in vivo recordings to test the sex differences in synaptic plasticity in the MDT-dmPFC circuit. We unilaterally injected AAV2/9-hSvnoChIEF, a variant of ChR2 that can faithfully respond to 100-Hz stimulation (Figures 4A and 4B), 35,36 into the MDT of adult male and female mice and implanted an optrode in the dmPFC to record field responses (Figure 4A). To compare the synaptic responses in the MDT-dmPFC pathway in male and female mice, we recorded field responses in the dmPFC evoked by photostimulation of the oChIEF-expressing MDT-dmPFC axonal terminals. After acquiring a stable baseline of field excitatory postsynaptic potentials (fEPSPs), we then photostimulated MDT-dmPFC axonal terminals with an optical LTP (oLTP) protocol containing four high-frequency stimulations (HFSs, 100 Hz, 1 s), spaced 20 s apart (Figure 4B; see STAR Methods). This oLTP protocol induced a long-lasting increase in the amplitude of fEPSPs in the dmPFC of male (p = 0.0059, Wilcoxon matchedpairs signed rank test; Figure 4C), but not female, mice (p = 0.16; Figure 4D). These results suggest that female mice are less likely to form LTP at MDT-to-dmPFC synapses compared with male mice under the same conditions.

Greater excitability of PV neurons in the mPFC of female mice

In order to understand the neurobiological basis of sex difference in the ability to form LTP at MDT-dmPFC synapses, we investigated and compared the neuronal properties along this pathway between male and female mice. We unilaterally injected the MDT with AAV2/1-hSyn-Cre, a virus that can cross synapses anterogradely,³⁷ and injected AAV2/9-DIO-EYFP on the same side of the dmPFC to label the MDT-projected dmPFC neurons (Figure 5A). After 4 weeks of viral expression, whole-cell patchclamp recordings were performed from acutely isolated dmPFC brain slices to record the electrophysiological characteristics of the EYFP-positive neurons (Figure 5A). We successfully recorded 84 neurons in 15 mice (39 neurons from 7 female and 45 neurons from 8 male mice). In each sex, the number of action potentials elicited (induced spikes) over an interval of 500 ms was measured, as the current was varied in steps of 50 pA, from 0 to 400 pA (Figure 5B). Waveform features of the first spike evoked at the minimum current step were analyzed (Figure 5B). At first glance, female and male mice displayed the same number of depolarizing-current-induced spikes (p = 0.94, two-way repeated measure ANOVA; Bonferroni multiple comparisons; Figure 5C) or basic electrical properties, including resting membrane potential (RMP), input resistance (Rin), capacitance (Cm), and spike properties (such as threshold potential, half-width, and amplitude), when all neurons were pooled together (Figure S6A). However, when these neurons were divided into putative excitatory and inhibitory types, sexual dimorphism emerged (Figures 5D-5H, S6B, and S6C). MDT is known to project to both excitatory pyramidal neurons and inhibitory interneurons in the mPFC. 38,39 Among the 84 recorded neurons, 62 putative pyramidal (pPyr) cells and 22 putative fast-spiking interneurons (pINs) were identified based on their spike responsiveness (Cm), spike waveform (half-width), and spike frequency (cumulative spike number) (Figure 5D; see STAR Methods for details). Although pPyr neurons were similar in male and female mice (p = 0.15 for Cm, unpaired t test; p =0.84 for spikes induced by current injection, two-way repeated measure ANOVA; Bonferroni multiple comparisons; Figures 5E and 5F), female pINs exhibited smaller Cm (p = 0.018, unpaired t test; Figure 5G), which may allow faster membrane potential changes and greater excitability. Indeed, more spikes were evoked in female pINs than in male pINs under the same current injection protocol (p = 0.03, two-way repeated measure ANOVA; Bonferroni multiple comparisons; Figure 5H), supporting higher excitability of female pINs in the MDT-projected dmPFC.

Among the two major inhibitory interneurons in the dmPFC, PV, and somatostatin (SST), previous studies reported that MDT axons make more synapses onto PV neurons⁴⁰ and that PV, but not SST, neurons mediate MDT-driven feedforward inhibition in

(H) Inhibitory effect of 589-nm yellow light on eNpHR3.0-expressing dmPFC neurons. Representative current-clamp trace of *in vitro* slice recording from an eNpHR3.0-expressing dmPFC neuron, with or without 589-nm yellow light stimulation (left). Comparison of number of spikes recorded from eNpHR3.0-expressing dmPFC neurons before, during, or after photostimulation (right). Friedman test with Dunn's multiple comparisons test, n = 10. Error bars indicate \pm SEM. *p < 0.05; **p < 0.01; ****p < 0.001; ****p < 0.001; n.s., not significant.

See also Figures S2, S3, and S5 and Table S1.



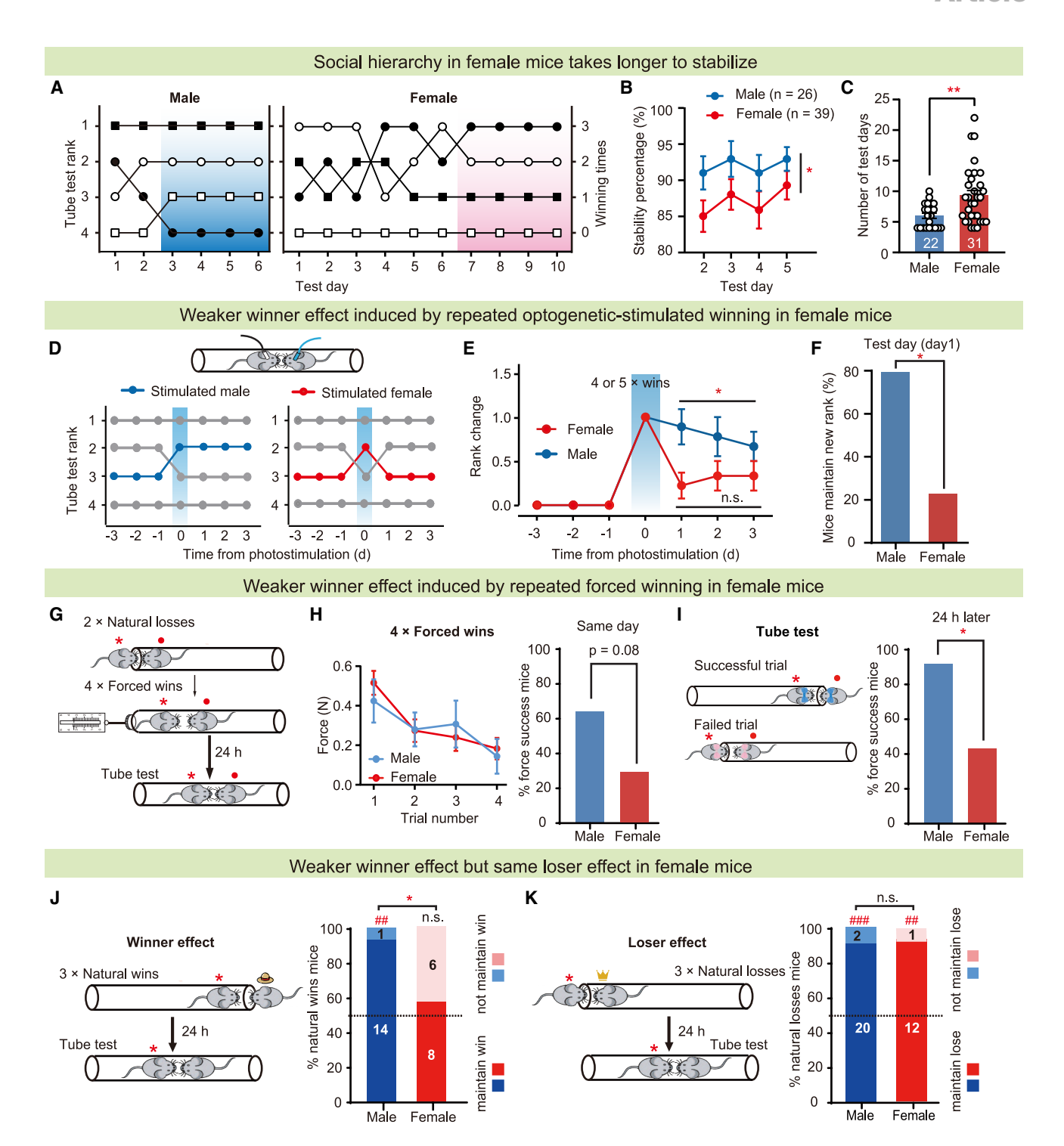


Figure 3. Weaker winner effect in female mice

(A) Example of rank positions in one cage of male (left) or female mice (right) from the first test day to the establishment of a stable hierarchy. Blue (male) and red (female) shadows represent mice maintained a stable hierarchy for 4 consecutive days.

- (B) Comparison of the stability percentage (percentage of mice maintaining the same rank as previous day) between male and female mice across 5 test days. n = 26 cages for males, n = 39 cages for females. Two-way repeated measure ANOVA.
- (C) Number of test days required to reach a stable hierarchy in male and female mice. n = 22 cages for males, n = 31 cages for females. Mann-Whitney test.
- (D) Daily tube test results for a cage of male (left) or female mice (right) before and after 4-5 dmPFC-photostimulated wins on day 0.
- (E) Average rank change of male and female mice before and after 4–5 dmPFC-photostimulated wins (n = 6 mice for 4 wins; n = 3 mice for 5 wins in both male and female groups). Wilcoxon signed rank test.

(legend continued on next page)



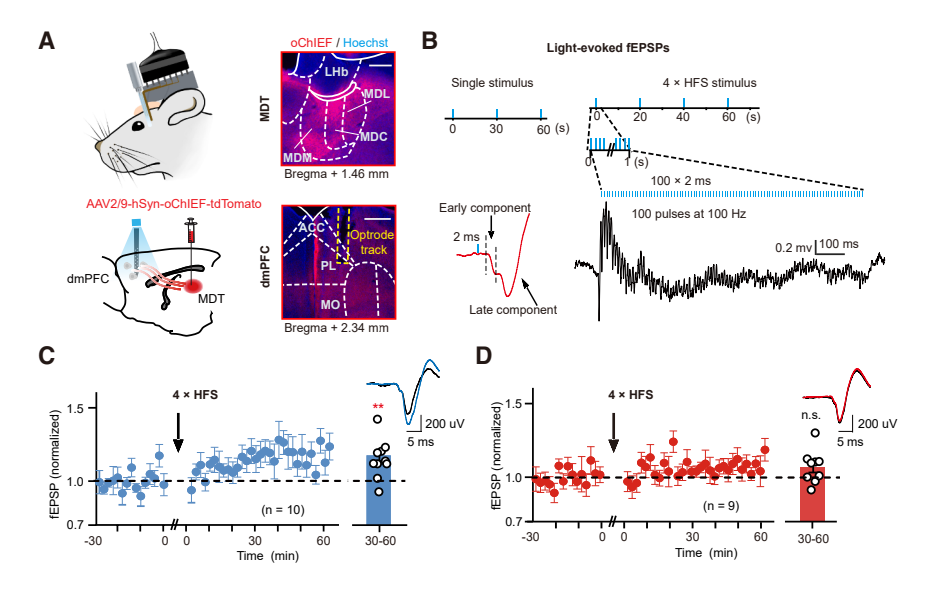


Figure 4. Reduced LTP in MDT-dmPFC circuit of female mice

(A) Left, schematic illustrating *in vivo* field recording, including viral construct, viral injection site, and optrode recording sites. Right, representative coronal section showing expression site of AAV2/9-oChIEF-tdTomato in the MDT (top). Representative coronal section showing tdTomato⁺ axonal terminals projected from the MDT and optrode placement site in the dmPFC (bottom). MDC, mediodorsal thalamus, central; MDM, mediodorsal thalamus, medial; MDL, mediodorsal thalamus, lateral; LHb, lateral habenula; MO, medial orbital cortex. Blue, Hoechst; red, tdTomato. Scale bars, 200 μm (top), 500 μm (bottom).

(B) Light-evoked fEPSP responses recorded in the dmPFC. Left, recording protocol for baseline and after oLTP (top). A light pulse elicits an fEPSP with clear early and delayed components. Right, oLTP protocols containing four HFSs (100 Hz, 1 s) to photostimulate the MDT-dmPFC pathway (top) and the corresponding fEPSP responses (bottom).

(C and D) Left, averaged slopes of normalized fEPSPs (average of four responses) before and after HFS for males (C) and females (D). Right, representative fEPSP traces before (black) and after (blue for male and red for female) HFS (top) and averaged slopes of normalized fEPSPs 30–60 min after HFS (bottom). Wilcoxon matched-pairs signed rank test.

Error bars indicate \pm SEM. **p < 0.01; n.s., not significant. See also Table S1.

the dorsal anterior cingulate cortex (dACC).38 We therefore next investigated which of these two interneuron types may be different in female mice (Figures 5I-5N, S6D, and S6E). We expressed the AAV2/9-DIO-EGFP virus in the dmPFC of PV-Cre (Figure 5I) or SST-Cre (Figure 5L) mice and made patch-clamp recording of GFP⁺ neurons. Female PV-INs displayed significantly smaller rheobase and greater Rin than male PV-INs (p < 0.0001 for rheobase, unpaired t test, p < 0.0001 for Rin, Mann-Whitney test; Figure 5J). In response to depolarizing step current injections, female PV-INs also exhibited a greater number of spikes (p < 0.0001, two-way repeated measure ANOVA; Bonferroni multiple comparisons; Figure 5K). Such differences were not found in SST-INs (p = 0.19 for rheobase, Mann-Whitney test; p = 0.74 for Rin, unpaired t test; p = 0.12 for induced spikes, two-way repeated measure ANOVA; Bonferroni multiple comparisons; Figures 5M and 5N). Together, these data indicate that PV, but not SST, neurons from the dmPFC of female mice are more excitable than those from males.

Increasing excitability of PV-INs in the dmPFC reduces LTP and the winner effect in male mice

We next tested whether the difference in excitability of PV-INs might contribute to the sexual dimorphisms in LTP within the MDT-dmPFC circuit and the behavioral winner effect. First, to specifically activate PV-INs, we unilaterally injected AAV expressing Cre-dependent NaChBac-a bacterial voltage-gated sodium channel-into the dmPFC of male PV-Cre mice to induce hyperexcitability (Figure 6A).41 Immunostaining confirmed the specificity of NaChBac expression in PV-INs (Figure 6B). Whole-cell recordings from acutely isolated dmPFC brain slices confirmed that, compared with EGFP control, NaChBac-expressing PV-INs had smaller rheobase (p = 0.0021, Mann-Whitney test; Figure 6C), indicating higher excitability. Indeed, NaChBac-expressing PV-INs showed more frequent spontaneous action potentials than EGFP-expressing ones (p = 0.022, Z test; Figure 6C). Although the same oLTP protocol as in Figure 4 induced a long-lasting increase in fEPSPs at MDT-to-mPFC synapses in male mice

Error bars indicate \pm SEM. *p < 0.05; **, ##p < 0.01; ###p < 0.001; n.s., not significant.

See also Figures S4 and S5 and Table S1.

⁽F) Percentage of male or female mice maintaining new rank position 1 day after dmPFC photostimulation (n = 6 mice for 4 wins; n = 3 mice for 5 wins in both male and female groups). Z test.

⁽G) Schematic of forced-win paradigm. Red star marks manipulated mouse and red dot marks opponent mouse.

⁽H) Average forces applied during each of the 4 forced-win trials (left) and percentage of mice maintaining new rank positions without exerting force (force success) at last forced-win trial (right). n = 11 for males, n = 14 for females, Z test.

⁽I) Schematic illustration of competition results (left) and percentage of mice maintaining new rank position on the following day (right). Red star marks manipulated mouse and red dot marks opponent mouse. n = 11 for males, n = 14 for females, Z test.

⁽J) Left, schematic of the "natural-win" paradigm. Red star marks the manipulated mouse, hat marks a weaker opponent, and unmarked mouse is naive opponent. Right, success rates against naive opponents on the following day after three natural wins against a weaker opponent. Success rates for each sex are also compared against chance level (50%). Number of animals is marked in the column. Z test (*); binomial test (#).

⁽K) Left, schematic of the "natural-loss" paradigm. Red star marks the manipulated mouse, crown marks a stronger opponent, and unmarked mouse is naive opponent. Right, failure rates against naive opponents on the following day after three natural losses against a stronger opponent. Failure rates for each sex are also compared against chance level (50 %). Number of animals is marked in the column. Z test (n.s.); binomial test (#).



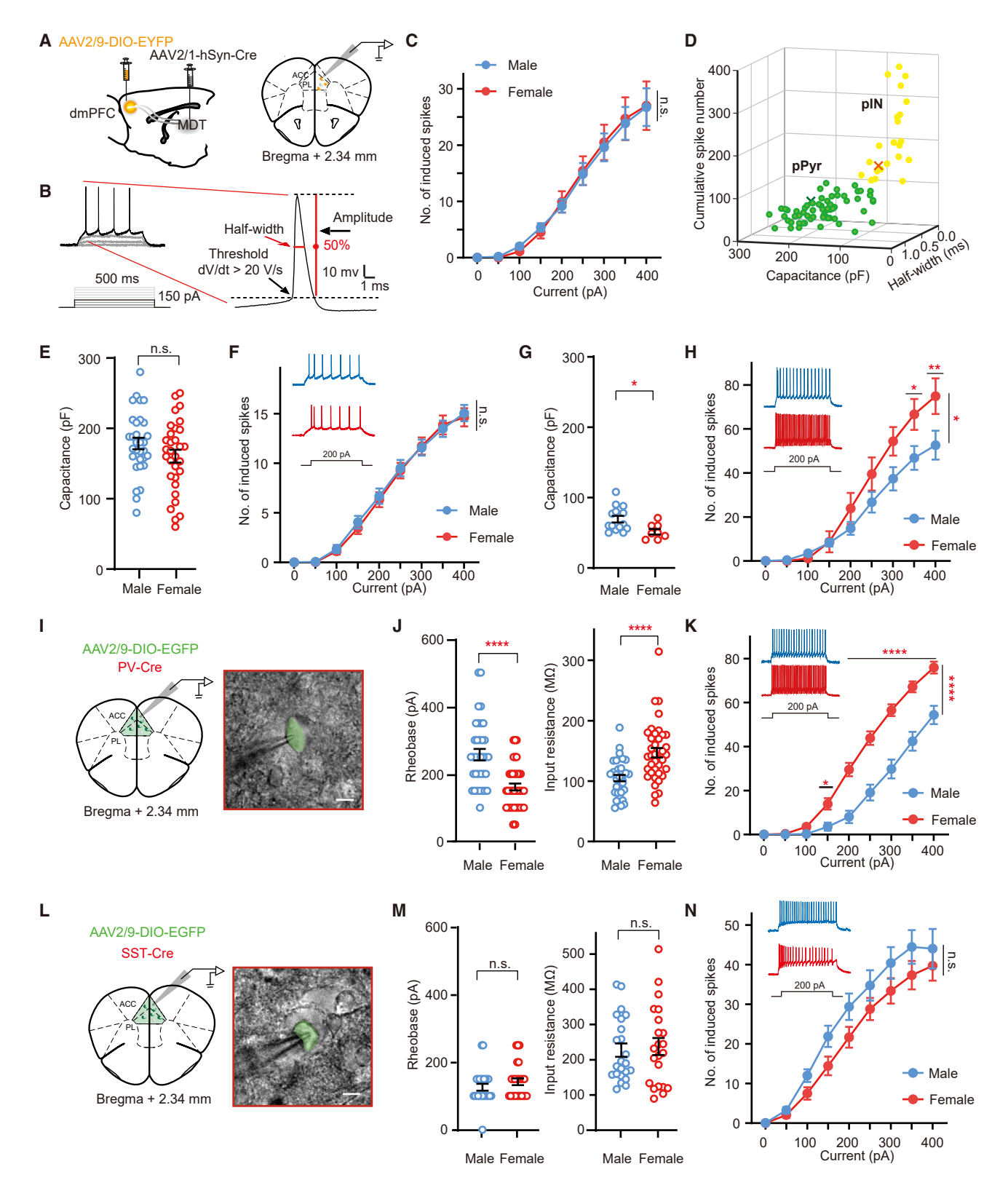


Figure 5. Greater excitability of PV neurons in the dmPFC of female mice

(A) Left, schematic illustrating the viral construct and viral injection site for in vitro electrophysiological recording. Right, schematic demonstrating electrode placement site in the dmPFC.



expressing the control EGFP virus, it failed to do so in male mice expressing NaChBac bilaterally in dmPFC PV-INs (p = 0.16 for NaChBac, p = 0.016 for EGFP, Wilcoxon matched-pairs signed rank test; p = 0.017 for EGFP versus NaChBac, unpaired t test, Figures 6D and 6E). Behaviorally, unlike the control mice, male mice expressing NaChBac bilaterally in the dmPFC were not able to maintain the winning status the day after the $3 \times$ natural wins, therefore showing a reduced winner effect (p > 0.99 for NaChBac, p = 0.023 for EGFP, binomial test; p = 0.089 for EGFP versus NaChBac, Z test; Figures 6F and 6G).

Decreasing excitability of PV-INs in the dmPFC induces LTP and increases the winner effect in female mice

We next tested whether suppressing excitability of PV-INs could induce LTP in the MDT-dmPFC circuit and, consequently, promote the formation of the winner effect in female mice. We achieved this by bilaterally injecting into the dmPFC of PV-Cre female mice AAV2/9-DIO-Kir2.1-EGFP, which expresses a Credependent inward-rectifying potassium channel (Kir2.1) that can persistently suppress neuronal excitability (Figure 7A). 41,42 Anatomically, we confirmed that Kir2.1 was specifically expressed in PV-INs (Figure 7B). Whole-cell recordings in Kir2.1-expressing dmPFC PV-INs revealed significantly increased rheobase and decreased spike numbers under current step injections, suggesting reduced excitability (p = 0.011 for rheobase, Mann-Whitney test; p = 0.0037 for induced spikes, two-way repeated measure ANOVA; Bonferroni multiple comparison test; Figure 7C). Although the same oLTP protocol as in Figure 4 did not induce a long-lasting increase in fEPSPs at MDT-to-mPFC synapses in female mice expressing the control EGFP, it was able to do so in female mice expressing Kir2.1 in dmPFC PV-INs (p = 0.031 for Kir2.1, p = 0.74 for EGFP, Wilcoxon matched-pairs signed rank test; p = 0.020 for EGFP versus Kir2.1, unpaired t test, Figures 7D and 7E). Behaviorally, female mice expressing Kir2.1 in dmPFC PV-INs were able to maintain their winning status the day after the $3 \times$ natural wins, therefore showing an increased winner effect (p = 0.021 for Kir2.1, p = 0.77 for EGFP, binomial test; p = 0.031 for EGFP versus Kir2.1, Z test; Figures 7F and 7G). These manipulation data suggest that the excitability of PV-INs causally underlies the sexually dimorphic effects on LTP induction in the MDT-dmPFC circuit, as well as the behavioral winner effect.

DISCUSSION

Here, we identified a neural circuit mechanism underlying the sexually dimorphic winner effect in mice, centered on PV-INs in the dmPFC. Female mice exhibited delayed social hierarchy formation and a weaker winner effect compared with males, correlating with reduced LTP at MDT-to-dmPFC synapses and heightened PV-IN excitability. Modulation experiments revealed that PV-IN activity controls LTP at MDT-to-dmPFC synapses and dominance behavior in a sex-dependent manner: increasing PV-IN excitability in male mice suppressed LTP and weakened the winner effect, whereas reducing PV-IN excitability in female mice enhanced LTP and promoted the winner effect. These findings point to a model in which elevated GABAergic inhibition from dmPFC local PV-INs raises the threshold for LTP induction in females, dampening the winner effect. This work identifies dmPFC PV-INs as a target for enhancing the winner effect and establishes a circuit-level framework for sex differences in competitive behaviors.

Social hierarchies in females

Many female mammals—such as degus, 43 bison, 44 caribou, 45 red deer, 46 vervet monkeys, 47 and chimpanzees 48 - can form dominance relationships during intrasexual competition for resources. In our study, virgin female C57BL/6J mice formed linear dominance hierarchies when competing for space (the tube), an ecologically relevant resource (Figure 1).49 This aligns with prior research showing that female mice in groups of 2-8 individuals can establish hierarchies based on tube test outcomes.^{28,50–53} However, results have been mixed in studies observing offensive and defensive behaviors in semi-natural enclosures, particularly when population densities are low. Notably, studies where females failed to form hierarchies^{54,55} typically had lower population densities than those where hierarchies were successfully established. 56-58 At the same population density, male laboratory mice and wild female mice, both of which exhibit robust aggression toward conspecifics, reliably form hierarchies.⁵⁵ These observations suggest that sufficient social interaction, facilitated by adequate population density, may be essential for establishing hierarchies among female mice, even in the absence of overt aggression.

(B) Left, schematic illustrating current injection protocol to induce spikes. Current was varied in steps of 50 pA from 0 to 400 pA. Right, schematic illustrating the criteria used to quantify waveform features, including threshold potential, half-width, and amplitude.

(C) Number of induced spikes at different current steps of all recorded dmPFC neurons in male (n = 45) and female mice (n = 39). Two-way repeated measure ANOVA; Bonferroni multiple comparisons post hoc tests.

(D) Clustering of all recorded dmPFC neurons (n = 84) in both sexes as pPyr (green, n = 62) neurons and pINs (yellow, n = 22) using κ -mean cluster-separation algorithm based on three electrophysiological properties: cumulative spike number, Cm, and half-width. "X" represents the centroid of each cluster.

(E and G) Cm of pPyr neurons (E, n = 31 neurons for males, n = 31 neurons for females) and pINs (G, n = 14 neurons for males, n = 8 neurons for females). Unpaired t test.

(F and H) Number of induced spikes of the pPyr neurons (F) and pINs (H) in male and female mice. Insets, representative traces at 200 pA depolarizing current. For males (blue) and females (red). Two-way repeated measure ANOVA; Bonferroni multiple comparisons post hoc tests.

(I and L) Left, schematics illustrating the viral construct and viral injection site in the PV-Cre (I) or SST-Cre (L) mice. Right, patch-clamp recording of PV-INs (I) or SST-INs (L) in the dmPFC under fluorescence microscopy. Scale bar, 20 µm.

(J and M) Rheobase and Rin in PV-INs (J, n = 34 for males, n = 38 for females) and SST-INs (M, n = 23 for males, n = 22 for females). Unpaired t test or Mann-Whitney test.



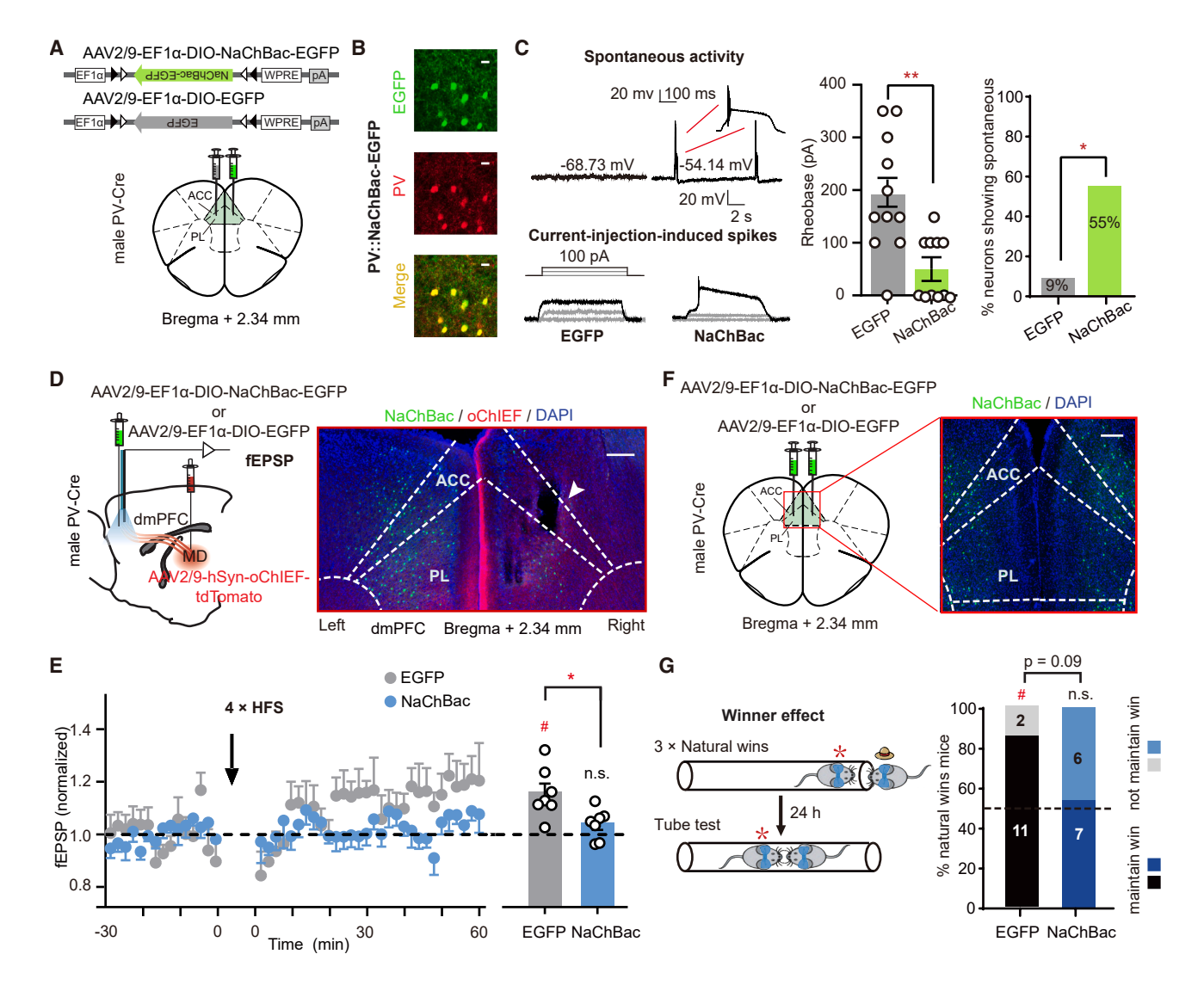


Figure 6. Increasing excitability of PV-INs in the dmPFC reduces LTP and the winner effect in male mice

(A) Schematics illustrating the AAV2/9-EF1 α -DIO-NaChBac-EGFP and AAV2/9-EF1 α -DIO-EGFP viral constructs and viral injection sites in the dmPFC of PV-Cre male mice. The two viruses were injected unilaterally into each side of the same mice for electrophysiology experiments in (C) and injected bilaterally for LTP and behavioral experiments in (D)–(G).

- (B) Immunostaining confirming the specificity of NaChBac-EGFP expression in PV-INs. Green, expressing NaChBac; red, expressing PV and yellow, expressing both. Scale bars, 20 μm.
- (C) Left, representative recording traces showing the spontaneous activity (top) and current-injection-induced spikes (bottom) of PV-INs expressing EGFP or NaChBac. Middle, rheobase in PV-INs expressing EGFP or NaChBac. Right, percentage of PV-INs expressing EGFP or NaChBac exhibited spontaneous firing. n = 11, 11, Mann-Whitney test for rheobase, Z test for percentage.
- (D) Schematic of *in vivo* oLTP recording showing the viral construct, viral injection, and optrode recording sites in PV-Cre males. Right, representative coronal section staining showing the expression of NaChBac-EGFP, tdTomato⁺ axonal terminals projected from the MDT, and the optrode placement site (indicated by the white arrowhead) in the dmPFC. Blue, DAPI; red, tdTomato; green, NaChBac. Scale bar, 200 μm.
- (E) Left, averaged slopes of normalized light-evoked fEPSPs (average of four responses) before and after HFS in PV-Cre male mice expressing EGFP or NaChBac-EGFP. Right, quantification of averaged slopes of normalized fEPSPs 30–60 min after $4 \times \text{HFS}$ in PV-Cre male mice (gray, EGFP, n = 7; blue, NaChBac-EGFP, n = 7), Wilcoxon matched-pairs signed rank test (#), unpaired t = 1 test (*).
- (F) Schematics illustrating the viral construct and viral injection site in the dmPFC of PV-Cre males for behavioral experiments. Right, representative coronal section staining showing the expression of the virus (green shading). Blue, DAPI; green, NaChBac-EGFP or EGFP. Scale bar, 200 µm.
- (G) Left, schematic of the natural-win paradigm in PV-Cre males. Red star marks the manipulated mouse, hat marks a weaker opponent, and unmarked mouse is naive. Right, success rates against naive opponents on the following day after three natural wins against a weaker opponent in PV-Cre male mice expressing EGFP or NaChBac-EGFP in the dmPFC. Success rates for each sex are also compared against chance level (50%). Number of animals is marked in the column. Z test (p = 0.09); binomial test (#).

Error bars indicate \pm SEM. *,#p < 0.05; n.s., not significant.

See also Table S1.



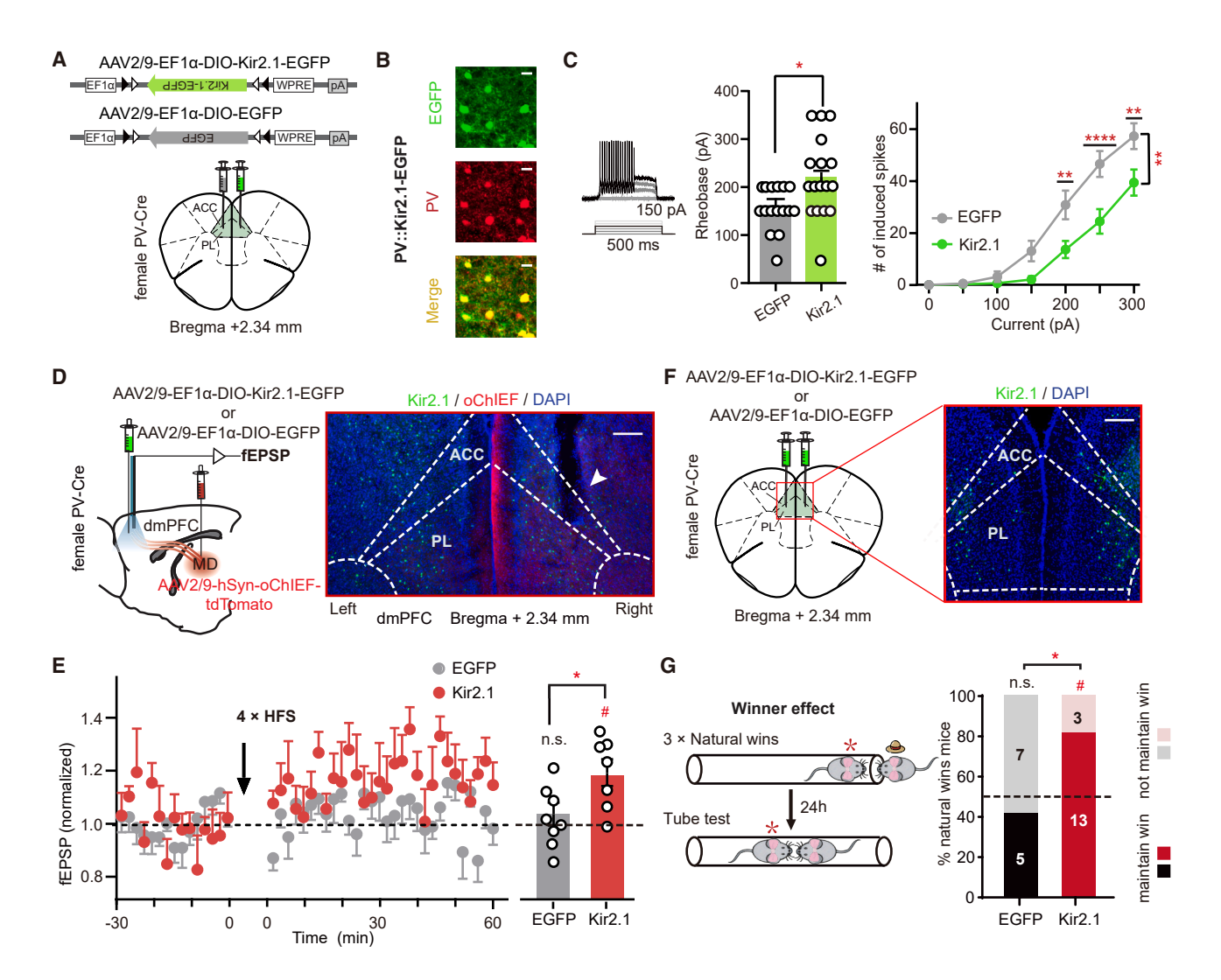


Figure 7. Decreasing excitability of PV-INs in the dmPFC induces LTP and the winner effect in female mice

(A) Schematics illustrating the AAV2/9-EF1α-DIO-Kir2.1-EGFP and AAV2/9-EF1α-DIO-EGFP viral constructs and viral injection sites in the dmPFC of PV-Cre female mice. The two viruses were injected unilaterally into each side of the same mice for electrophysiology experiments in (C) and injected bilaterally for LTP and behavioral experiments in (D)–(G).

(B) Immunostaining confirming the specificity of Kir2.1-EGFP expression in PV-INs. Green, expressing Kir2.1; red, expressing PV; and yellow, expressing both. Scale bars, 20 µm.

(C) Left, schematics illustrating current injection protocol to induce spikes and representative traces of depolarizing current. Current was varied in steps of 50 pA from 0 to 250 pA. Middle, rheobase of PV-INs expressing EGFP or Kir2.1. Right, number of induced spikes recorded at different depolarizing currents in PV-INs expressing EGFP (n = 16) or Kir2.1 (n = 17) in female mice. Mann-Whitney test for rheobase, Two-way repeated measure ANOVA, Bonferroni multiple comparisons post hoc tests for induced spikes.

(D) Schematic of *in vivo* oLTP recording showing the viral construct, viral injection, and optrode recording sites in PV-Cre females. Right, representative coronal section staining showing the expression of Kir2.1-EGFP, tdTomato⁺ axonal terminals projected from the MDT, and the optrode placement site (indicated by the white arrowhead) in the dmPFC. Blue, Hoechst; red, tdTomato; green, Kir2.1. Scale bars, 200 μm.

(E) Left, average slopes of normalized light-evoked fEPSPs (average of four responses) before and after HFS in PV-Cre female mice expressing EGFP or Kir2.1-EGFP. Right, quantification of averaged slopes of normalized fEPSPs 30–60 min after $4 \times HFS$ in PV-Cre female mice expressing EGFP or Kir2.1-EGFP (gray, EGFP, n = 8; red, Kir2.1, n = 7), Wilcoxon matched-pairs signed rank test (#), unpaired t test (*).

(F) Schematics illustrating the viral construct and viral injection site in the dmPFC of PV-Cre females for behavioral experiments. Right, representative coronal section staining showing the expression of the virus (green); blue, DAPI; green, Kir2.1-EGFP or EGFP. Scale bar, 200 μm.

(G) Left, schematic of the natural-win paradigm for PV-Cre females. Red star marks the manipulated mouse, hat marks a weaker opponent, and unmarked mouse is naive. Right, success rates against naive opponents on the following day after three natural wins against a weaker opponent in PV-Cre female mice expressing EGFP or Kir2.1-EGFP in the dmPFC. Success rates for each sex are also compared against chance level (50%). Number of animals is marked in the column. Z test (*): binomial test (#).

Error bars indicate \pm SEM. *,#p < 0.05, n.s., not significant. See also Table S1.





Recent studies have begun to explore the relationships between dominance rank and factors such as corticosterone levels, estrous state, and stress responses in female mice. 52,56-60 However, the neural mechanisms underlying social hierarchy formation in females remain understudied. Although specific cell types in the hypothalamic nuclei have been identified as promoting aggression in female mice, 61,62 our findings highlight the importance of the dmPFC in modulating social dominance in laboratory female mice (Figure 2). Future research should investigate the relationship between the hypothalamus and dmPFC, as well as other upstream and downstream circuits of the dmPFC involved in female social hierarchies, to determine whether similar behavioral phenotypes in males and females are regulated by distinct, sexually dimorphic neural circuits.

Sex differences in the winner effect

Our study reveals that female mice exhibited a weaker winner effect compared with males, requiring more trials to establish stable hierarchies and showing lower rank maintenance during hierarchy formation (Figures 3B and 3C). This was further supported by experiments involving external interventions (e.g., forced wins and optogenetic stimulation), which demonstrated that female mice were less likely to maintain newly acquired dominant ranks (Figures 3E, 3F, 3H, and 3I). Although the winner effect was weaker in female mice, the loser effect was equivalent between sexes (Figures 3J and 3K). This asymmetry may provide a compelling neurobehavioral explanation for delayed dominance hierarchy formation in females, as the reinforcing loop of repeated winning experiences—critical for stabilizing rank⁵—is less potent.

We would like to emphasize that this "weaker winner effect" in females does not translate into a tendency toward subordination. The finding here is about the reinforcement of winning, not an overall predisposition to lose. Instead, the "weak winner effect" in females may have evolutionary advantages. It may help reduce energy expenditure, minimize unnecessary conflicts, and allow for more flexible social status in dynamic environments, ultimately enhancing reproductive success. Rather than being maintained by the constant reinforcement of winswhich can create rigid, status-obsessed hierarchies - female social structures may be stabilized by factors like cooperation and consensus,63 with a neural bias that prevents a single victory from destabilizing group cohesion. Thus, sex differences in the winner effect may reflect complementary evolutionary specializations for navigating different social landscapes. These speculative interpretations, while derived from rodent models, invite future cross-species investigations.

The neural mechanisms underlying sex differences in the winner effect

Previous research on the neural mechanisms of the winner effect has primarily focused on males, revealing roles for synaptic plasticity in regions such as the lateral habenula, ⁶⁴ ventromedial hypothalamus, ^{6,65} and dmPFC. In our study, we found that female mice are less likely to form LTP at MDT-to-dmPFC synapses, potentially explaining their weaker winner effect in competitions (Figures 3 and 4). In addition, our *in vitro* electrophysiological re-

cordings revealed that PV-INs from female mice are more excitable compared with those from male mice (Figure 5). This is consistent with prior findings that female mice have higher PV-IN excitability in the prefrontal cortex.^{66,67} It is of interest to note that sex difference in the performance of spatial memory has also been attributed to a differential threshold for LTP induction in the hippocampal region,^{68,69} suggesting that, albeit involving different brain regions, sexually dimorphic behaviors may share similar cellular mechanisms.

Although neuromodulators (e.g., dopamine or endocannabinoids) or neurotrophic factors (e.g., brain-derived neurotrophic factor [BDNF]) can suppress local GABAergic activity to modulate LTP across brain areas, 70-72 the molecular basis for sex differences in mPFC PV-IN activity remains to be determined. For example, estrogen has been shown to increase PV-IN excitability in the rat barrel cortex, 73 whereas genetic deletion of metabotropic glutamate receptor subtype 5 (mGlu5) in PV-expressing cells eliminates sex differences in PV-IN physiology in the PFC.67 These findings imply that hormonal and synaptic signaling pathways may shape sex-dependent PV-IN function. Recent single-cell RNA sequencing studies have revealed numerous differentially expressed genes (DEGs) in mPFC PV-INs between males and females.⁷⁴ Future functional studies validating these DEGs could elucidate the molecular mechanisms by which PV-INs mediate sex-specific regulation of LTP and behavior.

By uncovering the sex-specific neural and circuit mechanisms underlying the winner effect, our study advances the understanding of how competitive behaviors and social hierarchies are regulated in males and females. These findings highlight the importance of considering sex as a biological variable in neuroscience research and provide a foundation for exploring how sex differences in neural plasticity shape competitive motivation and dominance behaviors.

RESOURCE AVAILABILITY

Lead contact

Requests for further information and resources should be directed to, and will be fulfilled by, the lead contact, Hailan Hu (huhailan@zju.edu.cn).

Materials availability

This study did not generate new unique reagents.

Data and code availability

- All data reported in this paper will be shared by the lead contact upon request.
- All original code has been deposited at https://doi.org/10.5281/zenodo. 17111667 and is publicly available as of the date of publication
- Any additional information required to reanalyze the data reported in this
 paper is available from the lead contact upon request.

ACKNOWLEDGMENTS

We thank Xiaoqi Wang, Jiayi Xu, Pinjie Li, Dou Li, Min Chen, Junying Wang, Tingting Zhou, Ligu Chen, Jiarui Chang, Yulin Li, Liqiang Wei, and colleagues from the Hu lab for assistance with experiments; Chunlei Zhang for advice on *in vitro* recording; Xinli Song and Kun Li for advice on biochemical experiments; Xiaohui Zhang and Xiang Yu for Cre mice; and Jing Xu and Bowen Tian for the DIY heating device. Some graphic components were created with BioRender.



This work was supported by the National Natural Science Foundation of China (32130042 and 82288101), the STI2030-Major Projects (2021ZD0203000 and 2021ZD0203001), the New Cornerstone Science Foundation, the Key R&D Program of Zhejiang (2024SSYS0016), the Fundamental Research Funds for the Central Universities (2025ZFJH01-01 and 226-2024-00087), the Non-profit Central Research Institute Fund of Chinese Academy of Medical Sciences (2023-PT310-01), and the Project for Hangzhou Medical Disciplines of Excellence and Key Project for Hangzhou Medical Disciplines (all to H.H.).

AUTHOR CONTRIBUTIONS

D.Z., S.J., Q.X., and A.Z. conducted the behavioral experiments, the optogenetic manipulation, and the related behavioral analysis. D.Z. performed the *in vivo* and *in vitro* electrophysiology experiments. D.Z. performed immunohistochemistry experiments with the assistance of S.J., X.J., and Y.T. H.H. and D. Z. designed the study. H.H. supervised the project and wrote the manuscript with D.Z. and Q.X.

DECLARATION OF INTERESTS

H.H. is a member of the advisory board of Neuron.

DECLARATION OF GENERATIVE AI AND AI-ASSISTED TECHNOLOGIES IN THE WRITING PROCESS

During the preparation of this work, the authors used ChatGPT to check grammar and spelling. After using this tool, the authors reviewed and edited the content as needed. No generative Al tools have been used to produce any new content. The authors take full responsibility for the content of the publication.

STAR*METHODS

Detailed methods are provided in the online version of this paper and include the following:

- KEY RESOURCES TABLE
- EXPERIMENTAL MODEL AND STUDY PARTICIPANT DETAILS
 - o Animals
- METHOD DETAILS
 - Behavioral assays
 - o Identification of the female estrous cycle
 - o Surgery and viral injection
 - o Behavioral manipulations
 - o In vivo electrophysiological recording of field potentials
 - o In vitro electrophysiological recording
- Histological verifications and immunohistochemistry
- QUANTIFICATION AND STATISTICAL ANALYSIS

SUPPLEMENTAL INFORMATION

Supplemental information can be found online at https://doi.org/10.1016/j.neuron.2025.09.029.

Received: February 12, 2025 Revised: August 1, 2025 Accepted: September 19, 2025

REFERENCES

 Hsu, Y., Earley, R.L., and Wolf, L.L. (2006). Modulation of aggressive behaviour by fighting experience: mechanisms and contest outcomes. Biol. Rev. Camb. Philos. Soc. 81, 33–74. https://doi.org/10.1017/ S146479310500686X.

- Tibbetts, E.A., Pardo-Sanchez, J., and Weise, C. (2022). The establishment and maintenance of dominance hierarchies. Philos. Trans. R. Soc. Lond. B Biol. Sci. 377, 20200450. https://doi.org/10.1098/rstb.2020.0450.
- Dugatkin, L.A. (1997). Winner and loser effects and the structure of dominance hierarchies. Behav. Ecol. 8, 583–587. https://doi.org/10.1093/beheco/8.6.583.
- Bonabeau, E., Theraulaz, G., and Deneubourg, J.L. (1999). Dominance orders in animal societies: the self-organization hypothesis revisited. Bull. Math. Biol. 61, 727–757. https://doi.org/10.1006/bulm.1999.0108.
- Zhou, T., Sandi, C., and Hu, H. (2018). Advances in understanding neural mechanisms of social dominance. Curr. Opin. Neurobiol. 49, 99–107. https://doi.org/10.1016/j.conb.2018.01.006.
- Yan, R., Wei, D., Varshneya, A., Shan, L., Dai, B., Asencio, H.J., Gollamudi, A., and Lin, D. (2024). The multi-stage plasticity in the aggression circuit underlying the winner effect. Cell 187, 6785–6803.e18. https://doi.org/ 10.1016/j.cell.2024.09.030.
- Page, L., and Coates, J. (2017). Winner and loser effects in human competitions. Evidence from equally matched tennis players. Evol. Hum. Behav. 38, 530–535. https://doi.org/10.1016/j.evolhumbehav.2017.02.003.
- Zhou, T., Zhu, H., Fan, Z., Wang, F., Chen, Y., Liang, H., Yang, Z., Zhang, L., Lin, L., Zhan, Y., et al. (2017). History of winning remodels thalamo-PFC circuit to reinforce social dominance. Science 357, 162–168. https://doi. org/10.1126/science.aak9726.
- Xiao, W., Jiao, Z.-L., Senol, E., Yao, J., Zhao, M., Zhao, Z.-D., Chen, X., Cao, P., Fu, Y., Gao, Z., et al. (2022). Neural circuit control of innate behaviors. Sci. China Life Sci. 65, 466–499. https://doi.org/10.1007/s11427-021-2043-2.
- Hashikawa, K., Hashikawa, Y., Lischinsky, J., and Lin, D. (2018). The Neural Mechanisms of Sexually Dimorphic Aggressive Behaviors. Trends Genet. 34, 755–776. https://doi.org/10.1016/j.tig.2018.07.001.
- Yang, C.F., and Shah, N.M. (2014). Representing sex in the brain, one module at a time. Neuron 82, 261–278. https://doi.org/10.1016/j.neuron. 2014 03 029
- Dugatkin, L.A., and Druen, M. (2004). The social implications of winner and loser effects. Proc. Biol. Sci. 271, S488–S489. https://doi.org/10.1098/ rshl 2004 0235
- Dugatkin, L.A., and Earley, R.L. (2003). Group fusion: the impact of winner, loser, and bystander effects on hierarchy formation in large groups. Behav. Ecol. 14, 367–373. https://doi.org/10.1093/beheco/14.3.367.
- Franz, M., McLean, E., Tung, J., Altmann, J., and Alberts, S.C. (2015). Selforganizing dominance hierarchies in a wild primate population. Proc. Biol. Sci. 282, 20151512. https://doi.org/10.1098/rspb.2015.1512.
- Kura, K., Broom, M., and Kandler, A. (2015). Modelling Dominance Hierarchies Under Winner and Loser Effects. Bull. Math. Biol. 77, 927–952. https://doi.org/10.1007/s11538-015-0070-z.
- Wang, F., Kessels, H.W., and Hu, H. (2014). The mouse that roared: neural mechanisms of social hierarchy. Trends Neurosci. 37, 674–682. https:// doi.org/10.1016/j.tins.2014.07.005.
- Wang, F., Zhu, J., Zhu, H., Zhang, Q., Lin, Z., and Hu, H. (2011).
 Bidirectional Control of Social Hierarchy by Synaptic Efficacy in Medial Prefrontal Cortex. Science 334, 693–697. https://doi.org/10.1126/science.1209951.
- Li, S.W., Zeliger, O., Strahs, L., Báez-Mendoza, R., Johnson, L.M., McDonald Wojciechowski, A., and Williams, Z.M. (2022). Frontal neurons driving competitive behaviour and ecology of social groups. Nature 603, 661–666. https://doi.org/10.1038/s41586-021-04000-5.
- Padilla-Coreano, N., Batra, K., Patarino, M., Chen, Z., Rock, R.R., Zhang, R., Hausmann, S.B., Weddington, J.C., Patel, R., Zhang, Y.E., et al. (2022). Cortical ensembles orchestrate social competition through hypothalamic outputs. Nature 603, 667–671. https://doi.org/10.1038/s41586-022-04507-5.
- Lindenfors, P., and Tullberg, B.S. (2011).
 Evolutionary Aspects of Aggression: The Importance of Sexual Selection.
 In Advances in Genetics Aggression, R. Huber, D.L. Bannasch, and P. Brennan, eds.





- (Academic Press), pp. 7–22. https://doi.org/10.1016/B978-0-12-380858-5.00009-5.
- Stagkourakis, S., Spigolon, G., Williams, P., Protzmann, J., Fisone, G., and Broberger, C. (2018). A neural network for intermale aggression to establish social hierarchy. Nat. Neurosci. 21, 834–842. https://doi.org/10.1038/ s41593-018-0153-x.
- Gauriot, R., and Page, L. (2019). Does Success Breed Success? a Quasi-Experiment on Strategic Momentum in Dynamic Contests. Econ. J. 129, 3107–3136. https://doi.org/10.1093/ej/uez040.
- Smith, N.M.T., and Dukas, R. (2024). Winner and loser effects in humans: evidence from randomized trials. Anim. Behav. 207, 101–107. https://doi. org/10.1016/j.anbehav.2023.10.017.
- Cohen-Zada, D., Krumer, A., and Shtudiner, Z. (2017). Psychological momentum and gender. J. Econ. Behav. Organ. 135, 66–81. https://doi.org/10.1016/j.jebo.2017.01.009.
- Oyegbile, T.O., and Marler, C.A. (2005). Winning fights elevates testosterone levels in California mice and enhances future ability to win fights. Horm. Behav. 48, 259–267. https://doi.org/10.1016/j.yhbeh.2005.04.007.
- Silva, A.L., Fry, W.H.D., Sweeney, C., and Trainor, B.C. (2010). Effects of photoperiod and experience on aggressive behavior in female California mice. Behav. Brain Res. 208, 528–534. https://doi.org/10.1016/j.bbr. 2009.12.038.
- Hood, K.E., and Cairns, R.B. (1988). A developmental-genetic analysis of aggressive behavior in mice. II. Cross-sex inheritance. Behav. Genet. 18, 605–619. https://doi.org/10.1007/BF01082312.
- Van Den Berg, W.E., Lamballais, S., and Kushner, S.A. (2015). Sex-Specific Mechanism of Social Hierarchy in Mice. Neuropsychopharmacology 40, 1364–1372. https://doi.org/10.1038/npp.2014.319.
- Zipple, M.N., Chang Kuo, D., Meng, X., Reichard, T.M., Guess, K., Vogt, C. C., Moeller, A.H., and Sheehan, M.J. (2025). Competitive social feedback amplifies the role of early life contingency in male mice. Science 387, 81–85. https://doi.org/10.1126/science.adq0579.
- Schjelderup-Ebbe, T. (1922). Beiträge zur Sozialpsychologie des Haushuhns. [Observation on the social psychology of domestic fowls]. Z. Psychol. 88, 225–252.
- Boyden, E.S., Zhang, F., Bamberg, E., Nagel, G., and Deisseroth, K. (2005). Millisecond-timescale, genetically targeted optical control of neural activity. Nat. Neurosci. 8, 1263–1268. https://doi.org/10.1038/nn1525.
- Gradinaru, V., Thompson, K.R., and Deisseroth, K. (2008). eNpHR: a Natronomonas halorhodopsin enhanced for optogenetic applications. Brain Cell Biol. 36, 129–139. https://doi.org/10.1007/s11068-008-9027-6.
- Yan, J.L., Smith, N.M.T., Filice, D.C.S., and Dukas, R. (2024). Winner and loser effects: a meta-analysis. Anim. Behav. 216, 15–22. https://doi.org/ 10.1016/j.anbehav.2024.07.014.
- Bégin, J., Beaugrand, J.P., and Zayan, R. (1996). Selecting dominants and subordinates at conflict outcome can confound the effects of prior dominance or subordination experience. Behav. Processes 36, 219–226. https://doi.org/10.1016/0376-6357(95)00031-3.
- Lin, J.Y., Lin, M.Z., Steinbach, P., and Tsien, R.Y. (2009). Characterization of engineered channelrhodopsin variants with improved properties and kinetics. Biophys. J. 96, 1803–1814. https://doi.org/10.1016/j.bpj.2008. 11.034.
- Nabavi, S., Fox, R., Proulx, C.D., Lin, J.Y., Tsien, R.Y., and Malinow, R. (2014). Engineering a memory with LTD and LTP. Nature 511, 348–352. https://doi.org/10.1038/nature13294.
- Zingg, B., Chou, X.-L., Zhang, Z.-G., Mesik, L., Liang, F., Tao, H.W., and Zhang, L.I. (2017). AAV-Mediated Anterograde Transsynaptic Tagging: Mapping Corticocollicular Input-Defined Neural Pathways for Defense Behaviors. Neuron 93, 33–47. https://doi.org/10.1016/j.neuron.2016.11.045.
- Delevich, K., Tucciarone, J., Huang, Z.J., and Li, B. (2015). The Mediodorsal Thalamus Drives Feedforward Inhibition in the Anterior Cingulate Cortex via Parvalbumin Interneurons. J. Neurosci. 35, 5743– 5753. https://doi.org/10.1523/JNEUROSCI.4565-14.2015.

- Li, F., Zheng, X., Wang, H., Meng, L., Chen, M., Hui, Y., Liu, D., Li, Y., Xie, K., Zhang, J., et al. (2024). Mediodorsal thalamus projection to medial prefrontal cortical mediates social defeat stress-induced depression-like behaviors. Neuropsychopharmacology 49, 1318–1329. https://doi.org/10. 1038/s41386-024-01829-y.
- Xiao, H., Xi, K., Wang, K., Zhou, Y., Dong, B., Xie, J., Xie, Y., Zhang, H., Ma, G., Wang, W., et al. (2024). Restoring the Function of Thalamocortical Circuit Through Correcting Thalamic Kv3.2 Channelopathy Normalizes Fear Extinction Impairments in a PTSD Mouse Model. Adv. Sci. (Weinh) 11, e2305939. https://doi.org/10.1002/advs.202305939.
- Lin, C.-W., Sim, S., Ainsworth, A., Okada, M., Kelsch, W., and Lois, C. (2010). Genetically Increased Cell-Intrinsic Excitability Enhances Neuronal Integration into Adult Brain Circuits. Neuron 65, 32–39. https://doi.org/10.1016/j.neuron.2009.12.001.
- Rothwell, P.E., Fuccillo, M.V., Maxeiner, S., Hayton, S.J., Gokce, O., Lim, B.K., Fowler, S.C., Malenka, R.C., and Südhof, T.C. (2014). Autism-Associated Neuroligin-3 Mutations Commonly Impair Striatal Circuits to Boost Repetitive Behaviors. Cell 158, 198–212. https://doi.org/10.1016/j. cell 2014 04 045
- Correa, L.A., Frugone, M.J., and Soto-Gamboa, M. (2013). Social dominance and behavioral consequences of intrauterine position in female groups of the social rodent *Octodon degus*. Physiol. Behav. *119*, 161–167. https://doi.org/10.1016/j.physbeh.2013.06.002.
- Rutberg, A.T. (1986). Dominance and Its Fitness Consequences in American Bison Cows. Behaviour 96, 62–91. https://doi.org/10.1163/ 156853986X00225.
- Barrette, C., and Vandal, D. (1986). Social rank, dominance, antler size, and access to food in snow-bound wild woodland caribou. Behaviour 97, 118–145. https://doi.org/10.1163/156853986X00342.
- Ceacero, F., García, A.J., Landete-Castillejos, T., Bartošová, J., Bartoš, L., and Gallego, L. (2012). Benefits for dominant red deer hinds under a competitive feeding system: food access behavior, diet and nutrient selection. PLoS One 7, e32780. https://doi.org/10.1371/journal.pone.0032780.
- Whitten, P.L. (1983). Diet and dominance among female vervet monkeys (Cercopithecus aethiops). Am. J. Primatol. 5, 139–159. https://doi.org/ 10.1002/ajp.1350050205.
- Murray, C.M., Eberly, L.E., and Pusey, A.E. (2006). Foraging strategies as a function of season and rank among wild female chimpanzees (Pan troglodytes). Behav. Ecol. 17, 1020–1028. https://doi.org/10.1093/beheco/ arl042.
- Fan, Z., Zhu, H., Zhou, T., Wang, S., Wu, Y., and Hu, H. (2019). Using the tube test to measure social hierarchy in mice. Nat. Protoc. 14, 819–831. https://doi.org/10.1038/s41596-018-0116-4.
- Smith-Osborne, L., Duong, A., Resendez, A., Palme, R., and Fadok, J.P. (2023). Female dominance hierarchies influence responses to psychosocial stressors. Curr. Biol. 33, 1535–1549.e5. https://doi.org/10.1016/j.cub.2023.03.020
- Varholick, J.A., Bailoo, J.D., Palme, R., and Würbel, H. (2018). Phenotypic variability between Social Dominance Ranks in laboratory mice. Sci. Rep. 8, 6593. https://doi.org/10.1038/s41598-018-24624-4.
- LeClair, K.B., Chan, K.L., Kaster, M.P., Parise, L.F., Burnett, C.J., and Russo, S.J. (2021). Individual history of winning and hierarchy landscape influence stress susceptibility in mice. eLife 10, e71401. https://doi.org/ 10.7554/eLife.71401.
- Fulenwider, H.D., Zhang, Y., and Ryabinin, A.E. (2024). Characterization of social hierarchy formation and maintenance in same-sex, group-housed male and female C57BL/6 J mice. Horm. Behav. 157, 105452. https:// doi.org/10.1016/j.yhbeh.2023.105452.
- Weidt, A., Gygax, L., Palme, R., Touma, C., and König, B. (2018). Impact of male presence on female sociality and stress endocrinology in wild house mice (Mus musculus domesticus). Physiol. Behav. 189, 1–9. https://doi. org/10.1016/j.physbeh.2018.02.039.



- Zilkha, N., Chuartzman, S.G., Sofer, Y., Pen, Y., Cum, M., Mayo, A., Alon, U., and Kimchi, T. (2023). Sex-dependent control of pheromones on social organization within groups of wild house mice. Curr. Biol. 33, 1407–1420. e4. https://doi.org/10.1016/j.cub.2023.02.039.
- Schuhr, B. (1987). Social structure and plasma corticosterone level in female albino mice. Physiol. Behav. 40, 689–693. https://doi.org/10.1016/0031-9384(87)90269-1.
- 57. Williamson, C.M., Lee, W., DeCasien, A.R., Lanham, A., Romeo, R.D., and Curley, J.P. (2019). Social hierarchy position in female mice is associated with plasma corticosterone levels and hypothalamic gene expression. Sci. Rep. 9, 7324. https://doi.org/10.1038/s41598-019-43747-w.
- Karamihalev, S., Brivio, E., Flachskamm, C., Stoffel, R., Schmidt, M.V., and Chen, A. (2020). Social dominance mediates behavioral adaptation to chronic stress in a sex-specific manner. eLife 9, e58723. https://doi. org/10.7554/eLife.58723.
- Davis, E.S., and Marler, C.A. (2004). c-fos Changes following an aggressive encounter in female California mice: a synthesis of behavior, hormone changes and neural activity. Neuroscience 127, 611–624. https://doi.org/10.1016/i.neuroscience.2004.05.034.
- Hyde, J., and Sawyer, T.F. (1977). Estrous cycle fluctuations in aggressiveness of house mice. Horm. Behav. 9, 290–295. https://doi.org/10.1016/0018-506x(77)90064-2.
- Sofer, Y., Zilkha, N., Gimpel, E., Wagner, S., Chuartzman, S.G., and Kimchi, T. (2024). Sexually dimorphic oxytocin circuits drive intragroup social conflict and aggression in wild house mice. Nat. Neurosci. 27, 1565– 1573. https://doi.org/10.1038/s41593-024-01685-5.
- Hashikawa, K., Hashikawa, Y., Tremblay, R., Zhang, J., Feng, J.E., Sabol, A., Piper, W.T., Lee, H., Rudy, B., and Lin, D. (2017). Esr1+ cells in the ventromedial hypothalamus control female aggression. Nat. Neurosci. 20, 1580–1590. https://doi.org/10.1038/nn.4644.
- Silk, J.B. (2007). Social Components of Fitness in Primate Groups. Science 317, 1347–1351. https://doi.org/10.1126/science.1140734.
- Chou, M.-Y., Amo, R., Kinoshita, M., Cherng, B.-W., Shimazaki, H., Agetsuma, M., Shiraki, T., Aoki, T., Takahoko, M., Yamazaki, M., et al. (2016). Social conflict resolution regulated by two dorsal habenular subregions in zebrafish. Science 352, 87–90. https://doi.org/10.1126/science.aac9508.
- Stagkourakis, S., Spigolon, G., Liu, G., and Anderson, D.J. (2020).
 Experience-dependent plasticity in an innate social behavior is mediated by hypothalamic LTP. Proc. Natl. Acad. Sci. USA 117, 25789–25799. https://doi.org/10.1073/pnas.2011782117.
- Jones, A.F., and Sheets, P.L. (2020). Sex-Specific Disruption of Distinct mPFC Inhibitory Neurons in Spared-Nerve Injury Model of Neuropathic Pain. Cell Rep. 31, 107729. https://doi.org/10.1016/j.celrep.2020.107729.
- Fabian, C.B., Jordan, N.D., Cole, R.H., Carley, L.G., Thompson, S.M., Seney, M.L., and Joffe, M.E. (2024). Parvalbumin interneuron mGlu5 receptors govern sex differences in prefrontal cortex physiology and binge

- drinking. Neuropsychopharmacology 49, 1861–1871. https://doi.org/10.1038/s41386-024-01889-0.
- Le, A.A., Lauterborn, J.C., Jia, Y., Wang, W., Cox, C.D., Gall, C.M., and Lynch, G. (2022). Prepubescent female rodents have enhanced hippocampal LTP and learning relative to males, reversing in adulthood as inhibition increases. Nat. Neurosci. 25, 180–190. https://doi.org/10.1038/ s41593-021-01001-5.
- Wang, W., Le, A.A., Hou, B., Lauterborn, J.C., Cox, C.D., Levin, E.R., Lynch, G., and Gall, C.M. (2018). Memory-Related Synaptic Plasticity Is Sexually Dimorphic in Rodent Hippocampus. J. Neurosci. 38, 7935– 7951. https://doi.org/10.1523/JNEUROSCI.0801-18.2018.
- Lu, H., Cheng, P.L., Lim, B.K., Khoshnevisrad, N., and Poo, M.M. (2010).
 Elevated BDNF after Cocaine Withdrawal Facilitates LTP in Medial Prefrontal Cortex by Suppressing GABA Inhibition. Neuron 67, 821–833. https://doi.org/10.1016/j.neuron.2010.08.012.
- Carlson, G., Wang, Y., and Alger, B.E. (2002). Endocannabinoids facilitate
 the induction of LTP in the hippocampus. Nat. Neurosci. 5, 723–724.
 https://doi.org/10.1038/nn879.
- Bissière, S., Humeau, Y., and Lüthi, A. (2003). Dopamine gates LTP induction in lateral amygdala by suppressing feedforward inhibition. Nat. Neurosci. 6, 587–592. https://doi.org/10.1038/nn1058.
- Clemens, A.M., Lenschow, C., Beed, P., Li, L., Sammons, R., Naumann, R. K., Wang, H., Schmitz, D., and Brecht, M. (2019). Estrus-Cycle Regulation of Cortical Inhibition. Curr. Biol. 29, 605–615.e6. https://doi.org/10.1016/j. cub.2019.01.045.
- Wang, Y., Song, X., Chen, X., Zhou, Y., Ma, J., Zhang, F., Wei, L., Qi, G., Yadav, N., Miao, B., et al. (2025). Integrating reproductive states and social cues in the control of sociosexual behaviors. Cell 188, 3530–3549.e24. https://doi.org/10.1016/j.cell.2025.04.035.
- Hippenmeyer, S., Vrieseling, E., Sigrist, M., Portmann, T., Laengle, C., Ladle, D.R., and Arber, S. (2005). A developmental switch in the response of DRG neurons to ETS transcription factor signaling. PLoS Biol. 3, e159. https://doi.org/10.1371/journal.pbio.0030159.
- Taniguchi, H., He, M., Wu, P., Kim, S., Paik, R., Sugino, K., Kvitsiani, D., Fu, Y., Lu, J., Lin, Y., et al. (2011). A Resource of Cre Driver Lines for Genetic Targeting of GABAergic Neurons in Cerebral Cortex. Neuron 71, 995–1013. https://doi.org/10.1016/j.neuron.2011.07.026.
- Friard, O., and Gamba, M. (2016). BORIS: a free, versatile open-source event-logging software for video/audio coding and live observations. Methods Ecol. Evol. 7, 1325–1330. https://doi.org/10.1111/2041-210X.12584.
- McLean, A.C., Valenzuela, N., Fai, S., and Bennett, S.A.L. (2012).
 Performing Vaginal Lavage, Crystal Violet Staining, and Vaginal Cytological Evaluation for Mouse Estrous Cycle Staging Identification.
 J. Vis. Exp. 4389, e4389, https://doi.org/10.3791/4389.
- Byers, S.L., Wiles, M.V., Dunn, S.L., and Taft, R.A. (2012). Mouse estrous cycle identification tool and images. PLoS One 7, e35538. https://doi.org/ 10.1371/journal.pone.0035538.





STAR*METHODS

KEY RESOURCES TABLE

REAGENT or RESOURCE	SOURCE	IDENTIFIER
Antibodies	5551.62	Serrice
Goat anti-rabbit Alexa Fluor 546	Invitrogen	Cat# A-11035; RRID: AB_143051
Rabbit anti-parvalbumin	Swant	Cat# PV 27; RRID: AB 2631173
Bacterial and virus strains	CWarn	Cat. 1 v 21,111 lb. 7 lb_2001110
AAV2/9-hSyn-eNpHR3.0-mCherry-	Taitool Bioscience, Shanghai	Cat# S0463-9
WPRE-pA	rancoi Biocolorico, changilar	Cath Co los C
AAV2/9-CAG-hChR2 (H134R)-tdTomato- WPRE-pA	Taitool Bioscience, Shanghai	Cat# S0168-9
AAV2/9-hSyn-mCherry-3Flag-WPRE-pA	Taitool Bioscience, Shanghai	Cat# S0238-9
AAV2/9-CAG-tdTomato-WPRE-pA	Taitool Bioscience, Shanghai	Cat#S1638-9-H30
scAAV2/1-hSyn-Cre-pA	Taitool Bioscience, Shanghai	Cat# S0292-1
AAV2/9-hSyn-oChIEF-tdTomato	OBIO Technology, Shanghai	Cat# AG50977
AAV2/9-Ef1α-DIO-EYFP	OBIO Technology, Shanghai	Cat# AG20296
AAV2/9-Ef1α-DIO-NaChBac-EGFP	OBIO Technology, Shanghai	Cat# H3302
AAV2/9-Ef1α-DIO-Kir2.1-P2A-EGFP- WPRE-hGH polyA	BrainVTA Technology, Wuhan	Cat# PT-1401
AAV2/9-Ef1α-DIO-EGFP-WPRE- hGH polyA	BrainVTA Technology, Wuhan	Cat# PT-0795
Chemicals, peptides, and recombinant protein	S	
Pentobarbital sodium	Sigma	Cat# P3761
Diff-Quik Staining kit	Phygene Scientific	Cat# LA1057
Experimental models: Organisms/strains		
Mouse: C57BL/6J	SLAC or GemPharmatech Laboratory animal, Shanghai	N/A
Mouse: PV-Cre	The Jackson Laboratory ⁷⁵	JAX. 008069; RRID:IMSR_JAX:008069
Mouse: SST-Cre	The Jackson Laboratory ⁷⁶	JAX. 013044; RRID:IMSR_JAX:013044
Software and algorithms		
OmniPlex neural recording data acquisition system	Plexon	https://plexon.com/products/omniplex- software; RRID: SCR_014803
NeuroExplorer	Plexon	https://plexon.com/products/ neuroexplorer; RRID: SCR_001818
pCLAMP10 software	Molecular Devices	https://www.moleculardevices.com/ products/axon-patch-clamp-system; RRID: SCR_011323
MultiClamp 700B amplifier	Molecular Devices	https://www.moleculardevices.com/ products/axon-patch-clamp-system; RRID: SCR_018455
DigiData 1550 digitizer	Molecular Devices	https://www.moleculardevices.com/ products/axon-patch-clamp-system; RRID: SCR_014270
MATLAB R2021a	MathWorks	https://www.mathworks.com/products/matlab.html; RRID: SCR_001622
Prism 8.0	GraphPad Software	https://www.graphpad.com/; RRID: SCR_002798
BORIS	Friard and Gamba ⁷⁷	http://www.boris.unito.it/; RRID: SCR_025700
ImageJ	National Institutes of Health	https://imagej.nih.gov/ij/index.html; RRID: SCR_003070
		(Continued on next page

(Continued on next page)

Neuron Article



Continued		
REAGENT or RESOURCE	SOURCE	IDENTIFIER
Any-maze	Stoelting	https://www.any-maze.com/; RRID: SCR_014289
Deposited data		
Custom analysis code	This paper	https://github.com/qqqaaazxz1996/Animal (https://doi.org/10.5281/zenodo.17111667)
Other		
473-nm and 589-nm laser LED	Inper, China	https://www.inper.com

EXPERIMENTAL MODEL AND STUDY PARTICIPANT DETAILS

Animals

Adult male and female C57BL/6J (8-24 weeks of age, SLAC or GemPharmatech Laboratory animal, Shanghai), PV-Cre (8-24 weeks of age, B6;129P2-Pvalbtm1(cre)Arbr/J, The Jackson Laboratory, JAX.008069)⁷⁵ and SST-Cre mice (8-13 weeks of age, STOCK Ssttm2.1(cre)Zjh/J, The Jackson Laboratory, JAX.013044)⁷⁶ were used for experiments. Mice of the same sex were housed in groups of 4 under standard housing conditions (12-h light/dark cycle with food and water ad libitum). All experiments were performed using age- and sex-matched mice. Animal care and all experimental procedures were performed under the guidelines of the Animal Care and Use Committee of Zhejiang University.

METHOD DETAILS

Behavioral assays

Tube test

The tube test assay was performed as previously described. ⁴⁹ A 30-cm long transparent tube with a 3.0-cm inside diameter allowed a single male mouse to pass through, while a similar tube with a 2.6-cm inside diameter accommodated a single female mouse. Before the tube tests, mice were trained to go through the tube in alternating directions for 10 trials per day for 2 days. In the following test days, mice were tested in pairs. Each pair of mice was simultaneously released from opposite ends of the tube. When the pair of mice met in the middle of the tube, the mouse that first retreated with four paws out of the tube was designated as the "loser", and the other mouse was designated as the "winner". The rank of each mouse was determined by the total number of wins on each test day. Social status was defined as stable only when mice maintained the same intra-cage rank position across 4 consecutive daily trials.

Using frame-to-frame video annotation, we identified three types of behaviors during each tube test competition: push (one mouse shoves its head under another mouse), resistance (maintaining position while being pushed, often with the head being pushed up), and retreat (backing out after being pushed or voluntarily withdrawing, often characterized by bending down of head). These behavior epochs were manually annotated and marked using the BORIS software.⁷⁷

Warm spot test

The warm spot test was applied as previously described. A rectangular plastic test box ($28 \,\mathrm{cm} \times 20 \,\mathrm{cm}$) was placed on ice to cool its floor to 0 °C. A circular cardboard enclosure (designated as the warm spot) was placed at one corner of the test box, equipped with a subjacent heating coil to maintain the local temperature at $32^{\circ}C \pm 1^{\circ}C$. Temperatures of the cold floor and warm circular enclosure were monitored using an infrared thermometer. A circular enclosure with a diameter of $4.5 \,\mathrm{cm}$ and a height of $1.2 \,\mathrm{cm}$ could accommodate only a single adult female mouse. A cage of four female mice was first placed in a box on ice without the warm corner for 30 min to acclimate to the cold environment, and was then transferred to the test box where they competed for the warm corner. Behaviors of the four female mice in the test box were videotaped for 40 min. Behavioral analyses were restricted to the final 20 minutes of the test, during which at least 90% (36 out of 40) of the mice had visited the warm spot at least once. BORIS software 77 was used to annotate the timestamps for both squeezing into and being squeezed out of the circular enclosure for each mouse, and the total duration of warm spot occupation was calculated as the cumulative time spent inside the enclosure. In the case where two mice stacked on top of each other, occupation duration was recorded for both mice. The tube test ranks of the mice were blinded to the experimenter performing the behavioral annotation.

"Forced win" paradigm

After two days of the tube test training, we randomly divided four cagemates into two pairs, ensuring that the weight difference within each pair was less than 10%. Then, we performed the tube test twice, with alternating directions, to identify the subordinate mice that consistently lost in both trials. Subsequently, we forced the subordinate mice to win against their dominant opponents four times by blocking the opponents' side of the tube. The tube blocker was connected to a dynamometer, which measured the force generated by subordinate mice during retreat. On the following day, tube test was conducted twice, with alternating directions, without the tube blocker to assess whether the original subordinate mice could win. When the results of the two trials were consistent (which was true in 80% of cases), they were included in the statistics.





"Natural win" paradigm

Mice were trained to go through the tube for 2 days as described above before the "natural win" test. On the first testing day, four mice from one cage each achieved three wins against subordinate mice from other cages, which had previously experienced at least two losses in tube tests. Trials lasting less than 3 seconds were excluded. In the second cage of naïve mice, all four mice went through the tube individually without encountering opponents for three trials. On the second testing day, we randomly paired each mouse that had achieved three wins on the first testing day with a naïve mouse (weight differences < 10%) from the other cage, and conducted the tube test twice to assess the winner effect. When the results of the two trials were consistent (which was true in 85% of cases), they were included in the statistics.

In the experiments concerning the estrous cycle in the "natural win" test, we incorporated vaginal smear sampling into the behavioral protocol. To minimize potential interference to subsequent behavioral tests, female mice were acclimated to the sampling procedure three consecutive days preceding the "natural win" test, and vaginal smears were collected at least 2 hours before the tube test on the first testing day. To investigate whether the estrous cycle affects the winner effect, female mice were divided into four groups corresponding to their estrous cycle stages.

"Natural loss" paradigm

Mice were trained to go through the tube for 2 days as described above before the "natural loss" test. On the first testing day, four mice from one cage each achieved three losses against dominant mice from other cages, which had previously experienced at least two wins in tube tests. Trials lasting less than 3 seconds were excluded. In the second cage of naïve mice, all four mice went through the tube individually without encountering opponents for three trials. On the second testing day, we randomly paired each mouse that had experienced three losses on the first testing day with a naïve mouse (weight differences < 10%) from the other cage, and conducted the tube test twice to assess the loser effect. When the results of the two trials were consistent (which was true in 94% of cases), they were included in the statistics.

Identification of the female estrous cycle

The estrous cycle of female mice is divided into four stages: proestrus, estrus, metestrus, and diestrus, which can be determined by cytological evaluation of vaginal smears according to the published literature. 78,79 To collect vaginal smears, each female mouse was securely restrained by gently grasping the skin at the nape and back. The vaginal opening was rinsed with sterile ddH₂O using a 100 μ l pipette. Then, the pipette tip preloaded with approximately 20 μ l of sterile ddH₂O was positioned at the opening and gently flushed by aspirating and releasing the solution 4–6 times to collect the lavage solution containing exfoliated cells. It is worth noting that the pipette tip should never be inserted into the vaginal canal to avoid the effect of vaginal stimulation.

The vaginal smears were dried on slides and stained with Diff-Quik Stain Kit (Phygene Scientific) to determine the estrous cycle. The estrous cycle stages were determined as follows: proestrus, characterized by round, uniform nucleated epithelial cells; estrus, characterized by exclusively cornified epithelial cells; metestrus, characterized by mixed cornified epithelial cells and leukocytes; and diestrus, characterized by abundant leukocytes with few nucleated epithelial cells (Figure S4B).

Surgery and viral injection

After being anesthetized with 1% sodium pentobarbital (100 mg/kg body weight), mice were head-fixed in a stereotaxic frame (RWD Instruments). A glass pipette connected to a pressure microinjector (Picospritzer III, Parker) was used to deliver the virus (0.2 μ l per site) to the target brain regions.

For optogenetic activation of the dmPFC, AAV2/9-CAG-hChR2 (H134R)-tdTomato (titer: 1.32×10^{13} v.g./ml, diluted 1:5, Taitool Bioscience) or the control virus AAV2/9-CAG-tdTomato- WPRE-pA (titer: 7.95×10^{12} v.g./ml, diluted 1:3, Taitool Bioscience) was injected into the right dmPFC (AP: + 2.43 mm from bregma, ML: + 0.4 mm from the midline, DV: - 1.2 mm from the dura), and a mono fiber-optic cannula (NA = 0.37, Newdoon Inc. or Inper Inc.) was implanted 300-400 μ m above the viral injection site. Fluorescence intensity was confirmed to be comparable between male and female mice.

For optogenetic inhibition of the dmPFC, AAV2/9-hSyn-eNpHR3.0-mCherry-WPRE-pA (titer: 1.76×10^{13} v.g./ml, diluted 1:5, Taitool Bioscience) or the control virus AAV2/9-hSyn-mCherry-WPRE-pA (titer: 2.49×10^{13} v.g./ml, diluted 1:8, Taitool Bioscience) was bilaterally injected into the dmPFC (AP: +2.43 mm from bregma, ML: \pm 0.6 mm from the midline, DV: -1.25 mm from the dura) at a 10° angle in the ML direction, and dual fiber-optic cannulae were implanted 300-400 μ m above the viral injection sites.

For *in vivo* recording the synaptic strength of the MDT-dmPFC pathway, AAV2/9-hSyn-oChIEF-tdTomato (titer: 1.75×10^{13} v.g./ml, diluted 1:5, OBIO Technology) was injected into the MDT (AP: - 1.50 mm from bregma, ML: + 0.43 mm from the midline, DV: - 3.35 mm from the dura). Fluorescence intensity was confirmed to be comparable between sexes.

For recording the electrophysiological characteristics of dmPFC neurons receiving projections from the MDT, transsynaptic virus scAAV2/1-hSyn-Cre (titer: 1.97×10^{13} v.g./ml, diluted 1:2, Taitool Bioscience) was injected into the ipsilateral MDT (AP: -1.50 mm from bregma, ML: + 0.43 mm from the midline, DV: -3.35 mm from the dura), and AAV2/9-Ef1 α -DIO-EYFP (titer: 4.2×10^{13} v.g./ml, diluted 1:10, OBIO Technology) was injected into the ipsilateral dmPFC (AP: + 2.43 mm from bregma, ML: + 0.4 mm from the midline, DV: - 1.2 mm from the dura).

Neuron Article



To compare the electrophysiological characteristics of PV and SST neurons in the dmPFC between males and females, AAV2/9-Ef1 α -DIO-EGFP-WPRE-hGH polyA (titer: 1.0 \times 10¹³ v.g./ml, diluted 1:5, BrainVTA Technology) was bilaterally injected into the dmPFC (AP: + 2.43 mm from bregma, ML: \pm 0.4 mm from the midline, DV: -1.2 mm from the dura) of male and female PV-Cre or SST-Cre mice, to specifically label PV and SST neurons.

For activation of PV-INs in the dmPFC of male mice, AAV2/9-Ef1 α -DIO-NaChBac-EGFP (titer: 1.21 \times 10¹³ v.g./ml, diluted 1:3, OBIO Technology) or the control virus AAV2/9-Ef1 α -DIO-EGFP-WPRE-hGH polyA (titer: 1.0 \times 10¹³ v.g./ml, diluted 1:5, BrainVTA Technology) was bilaterally injected into the dmPFC (AP: + 2.43 mm from bregma, ML: \pm 0.4 mm from the midline, DV: - 1.2 mm from the dura) of male PV-Cre mice.

For inhibition of PV-INs in the dmPFC of female mice, AAV2/9-Ef1 α -DIO-Kir2.1-P2A-EGFP-WPRE-hGH polyA (titer: 5×10^{12} v.g./ml, diluted 1:2, BrainVTA Technology) or the control virus AAV2/9-Ef1 α -DIO-EGFP-WPRE-hGH polyA (titer: 1.0×10^{13} v.g./ml, diluted 1:5, BrainVTA Technology) was bilaterally injected into the dmPFC (AP: + 2.43 mm from bregma, ML: \pm 0.4 mm from the midline, DV: - 1.2 mm from the dura) of female PV-Cre mice.

The glass pipette was withdrawn 10 min after injection. Optic fibers were secured onto the skull using dental cement. After surgery, mice were placed on a heating pad to recover from anesthesia. Mice were given at least one week to recover before behavioral testing.

Behavioral manipulations

Optogenetic manipulation of the dmPFC of female mice in tube test

For female mice implanted with optic connectors, a 12-mm slit was made at the top of the tube with a 2.6-cm inside diameter. All optogenetic manipulation experiments were conducted at least 4 weeks after viral injection to ensure full expression of ChR2 or eNpHR3.0. Only mouse cages with stable ranks (all mice maintained the same rank position for over 4 consecutive days) were used for further optogenetic manipulations. On the test day, subject mice were habituated to the fiber connection. Tube test ranks were reconfirmed under light-off conditions with other cagemates wearing fake optic fiber connectors. Then, 473-nm blue light (100 Hz, 9 ms per pulse, 4 pulses per second, for mice injected with ChR2) or 589-nm yellow light (constant, for mice injected with eNpHR3.0) was turned on just before the mice entered the tube. For each test mouse, we started light stimulation with 1 mW. A light intensity was considered effective if the test mouse won or lost from both ends of the tube, indicating a successful rank change. If a certain light intensity could not lead to a successful rank change, the light intensity would be increased gradually until a change in rank occurred or the laser reached the maximum intensity (30 mW for blue light; 15 mW for yellow light). We quantified the number of successful rank-change events (denoted as numbers in the "Day 0" box) induced by light stimulation in each test mouse in Figures S2A, S2B, and S4A, with "0" indicating no rank change after stimulation. These values represent successful events only and do not reflect the total number of stimulations. Tube tests on the test day were videotaped by a camera placed beside the tube for annotation, and the detailed behaviors of rank-changed trials were further compared between light-off and light-on conditions.

The optogenetic activation was effective for mice of different ranks, except for rank-1 mice, where a ceiling effect exists. Therefore, we excluded the results of rank-1 mice from the statistical analysis. Similarly, due to a floor effect, we excluded the results of rank-4 mice from the statistical analysis for optogenetic inhibition experiments. The data of female mice that won 4 or 5 trials during light stimulation was analyzed to compare with males in Figures 3E and 3F. To avoid repeated data usage, these data were excluded from the analyses in Figures 2D–2F. See Figure S5 for detailed information on rank changes and maintenance resulting from varying numbers of photoactivation (Figures S5A, S5B, and S5D) and photoinhibition (Figures S5A, S5C, and S5D) trials for each female subject.

Optogenetic manipulation of the dmPFC during open field test in female mice

Mice were individually placed in the center zone of open field $(40 \times 40 \text{ cm})$ chamber with dim light (5-10 lux) for 10 minutes. Their movements were recorded by a camera positioned directly above the arena and analyzed by Any-maze software (Stoelting). 589-nm yellow light (constant; 5 mW) or 473-nm blue light (100 Hz, 9 ms per pulse, 4 pulses per second; 10 mW) was intermittently turned on and off in 1-min epochs. Total distance was analyzed to evaluate the locomotion ability, and percentage of time spent in the center per minute was analyzed to assess the anxiety level.

Optogenetic manipulation of the dmPFC during elevated plus maze test in female mice

Mice were gently placed in the center of the maze, with their heads facing a close arm. Mice were allowed to freely explore the elevated plus maze for 9 minutes. A video camera positioned directly above the arena was used to track each mouse, and the data were analyzed using Any-maze software (Stoelting, U.S.). 589-nm yellow light (constant, 5 mW) or 473-nm blue light (100 Hz, 9 ms per pulse, 4 pulses per second; 10 mW) was intermittently turned on and off in 3-min epochs. Time spent in open arms was calculated to assess the anxiety level.

Manipulating the excitability of PV-INs in the dmPFC

We expressed AAV2/9-Ef1 α -DIO-NaChBac-EGFP into the bilateral dmPFC of male PV-Cre mice to activate PV-INs, and AAV2/9-Ef1 α -DIO-Kir2.1-EGFP in bilateral dmPFC of female PV-Cre mice to inhibit PV-INs. We also expressed AAV2/9-Ef1 α -DIO-EGFP in both males and females as a control. All mice in the same cage received injections of the same virus. Mice were given viral injections at least 4 weeks prior to behavioral manipulations to ensure full viral expression. To investigate how the excitability of PV-INs in the dmPFC affects the winner effect, we conducted behavioral manipulations under the "natural win" paradigm.





On the first testing day, each of the four mice in the same cage achieved three wins against subordinate mice from other cages, as described above. For the other cage of naïve mice injected with the same virus, all four mice individually went through the tube without encountering opponents for three trials.

On the second testing day, a mouse that had experienced three wins on the first day was randomly paired with a naïve opponent from the other cage (weight difference <10%), which had received the same virus. This experimental design ensured that, apart from the winning experience, there were no other differences between the paired mice. Each pair of mice underwent the tube test twice to validate the winner effect. When the results of the two trials were consistent (which was true in 77% of cases), they were included in the statistics.

In vivo electrophysiological recording of field potentials

To compare the synaptic strength of the MDT-dmPFC pathway between male and female mice, we recorded optical fEPSP in the dmPFC after injecting AAV2/9-hSyn-oChIEF-tdTomato into the MDT. To further examine how PV-IN excitability in the dmPFC influences synaptic strength, we injected the above virus into the MDT and additionally injected AAV2/9-Ef1α-DIO-NaChBac-EGFP into the bilateral dmPFC of male PV-Cre mice to activate PV-INs, whereas AAV2/9-Ef1α-DIO-Kir2.1-EGFP was injected into the bilateral dmPFC of female PV-Cre mice to inhibit PV-INs. We also expressed AAV2/9-Ef1α-DIO-EGFP both in males and females as a control.

Five weeks after viral injection, animals were anesthetized again with 1% sodium pentobarbital (100 mg/kg body weight) and fixed in a stereotaxic frame (RWD Instruments). The hand-made optrode consisted of four-channel nichrome electrodes and an optical fiber in the center (0.4 mm above the tip of the electrodes), which was lowered into the brain targeting the right dmPFC (AP: +2.43 mm from bregma, ML: +0.4 mm from the midline, DV: -1.2 mm from the dura). Mice were single-housed for 7 days for recovery after surgery and optical fEPSPs were then recorded in the homecage. For optical stimulation, the optical fiber was connected to a 473-nm laser. The laser power was adjusted to elicit an fEPSP with clear early and delayed components. 2-ms light pulses at 0.033 Hz were delivered to evoke fEPSPs. After a stable baseline was established for at least 30 minutes, optical high-frequency stimulation (HFS; four trains of 100 × 2-ms pulses at 100 Hz, 20-s inter-train interval) was delivered at the recording site, followed by fEPSP recordings for at least 2 hours. Each fEPSP was normalized to field potentials 10 ms before optical stimulation. The slope of the normalized fEPSP was calculated as previously described. All data were analyzed using a custom-written MATLAB program.

In vitro electrophysiological recording Slice preparation

Mice were anesthetized with 1% sodium pentobarbital (100 mg/kg i.p.) and then perfused with 20 mL ice-cold dissection buffer (220 mM sucrose, 2 mM KCl, 1.15 mM NaH_2PO_4 , 0.2 mM $CaCl_2$, 26 mM $NaHCO_3$, 6 mM $MgCl_2$ and 10 mM glucose, oxygenated with 95% O_2 and 5% CO_2). Brains were quickly dissected out after decapitation. Coronal slices (300 μ m in thickness) were prepared using a vibratome (VT1200S, Leica) in oxygenated chilled dissection buffer. The slices were then incubated in ACSF (125 mM $NaCl_3$, 2.5 mM $NaHCO_3$, 1.25 mM NaH_2PO_4 , 25 mM glucose, 1 mM $MgCl_2$, 2 mM $CaCl_3$ and 1 mM pyruvate, oxygenated with 95% O_2 and 5% CO_2) at 32-34°C for 1 hour to recover and subsequently maintained at room temperature.

Recording and data analysis

During recordings, slices were superfused with a physiological extracellular solution (125 mM NaCl, 2.5 mM KCl, 25 mM NaHCO₃, 1.25 mM NaH₂PO₄, 25 mM glucose, 1 mM MgCl₂ and 2 mM CaCl₂, oxygenated with 95% O₂ and 5% CO₂). Neurons were visualized with Olympus microscope (BX51W1) equipped with infrared differential interference contrast optics. Recordings were performed with a MultiClamp 700B amplifier controlled by DigiData 1550 digitizer and pCLAMP10 software (Axon Instruments). Whole-cell recording was performed with glass pipettes with a typical resistance of 4-6 $M\Omega$.

To test the function of the expressed eNpHR3.0 protein in the dmPFC, whole cell recordings were performed with glass pipettes filled with internal solution (150 mM K-Gluconate, 5 mM NaCl, 1 mM MgCl₂, 2 mM Mg-ATP, 0.5 mM Na-GTP, 0.2 mM EGTA and 10 mM HEPES, adjusted to pH 7.35 with KOH). Neurons expressing eNpHR3.0 were visually identified by tdTomato fluorescence. A constant 589-nm light of 2 mW intensity was delivered through a 200 μ m optical fiber positioned near the recorded region. Current-clamp recordings (I = 250 pA, 500 ms) were performed on eNpHR3.0-expressed dmPFC neurons to monitor light-induced inhibition of action potentials during intermittent photoinhibition (500-ms light on and off epochs).

To compare the excitability of dmPFC neurons receiving MDT projections between male and female mice, we labeled these neurons by injecting transsynaptic virus scAAV2/1-hSyn-Cre into the right MDT and AAV2/9-hEf1 α -DIO-EYFP into the right dmPFC of male and female mice. All the recorded neurons were classified into putative pyramidal (pPyr) neurons and inhibitory interneurons (pIN) using an unsupervised κ -means clustering algorithm. Three parameters—including cumulative firing numbers induced by various depolarizing currents (from 50 pA to 500 pA, 500-ms duration), capacitance and half-width of the action potential—were used for the analysis (Figure 5D).

To compare the excitability of PV and SST neurons in the dmPFC between male and female mice, we labeled PV or SST neurons by bilaterally injecting AAV2/9-Ef1 α -DIO-EGFP into the dmPFC of PV-Cre and SST-Cre mice. Recordings were performed in current-clamp mode (I = 0 pA) with a K-based internal solution (150 mM K-Gluconate, 5 mM NaCl, 1 mM MgCl₂, 2 mM Mg-ATP, 0.5 mM Na-GTP, 0.2 mM EGTA and 10 mM HEPES, adjusted to pH 7.35 with KOH). The resting membrane potential was recorded for 3 min, followed by stepwise depolarizing current steps from 0 pA to 400 pA in 50-pA increments. The number of action potentials evoked within a 500-ms window was also measured. Additionally, a 20-pA hyperpolarizing current was injected for 200 ms to





measure input resistance. Parameters such as membrane capacitance, input resistance, resting membrane potential, input-output current curves, rheobase current, action potential threshold, threshold voltage, half-width, and action potential amplitude were compared between male and female PV and SST neurons. To further examine whether NaChBac expression channel activates PV-INs, AAV2/9-Ef1 α -DIO-NaChBac-EGFP was injected into the dmPFC of male PV-Cre mice in one hemisphere, while AAV2/9-Ef1 α -DIO-EGFP was injected into the contralateral hemisphere as a control. Similarly, to examine whether Kir2.1 expression inhibits PV-INs, AAV2/9-Ef1 α -DIO-Kir2.1-EGFP was injected into one hemisphere of the dmPFC in female PV-Cre mice, while AAV2/9-Ef1 α -DIO-EGFP was injected into the contralateral hemisphere as a control. Neurons expressing EGFP were visually identified under a fluorescence microscopy, and whole-cell patch-clamp recordings were performed using a K-based internal solution. Resting membrane potential (RMP) was recorded in current-clamp mode (I = 0 pA) for 3 min. The neurons were then subjected to depolarizing current steps from 0 pA to 250 pA in 50-pA increments, and the number of action potentials evoked within a 500-ms window was also measured. Comparisons of resting membrane potential, rheobase current (the minimal current required to elicit an action potential), and the input-output current curve between neurons from the two hemispheres of the dmPFC were conducted.

Histological verifications and immunohistochemistry

Histology was performed to confirm the location of implanted optic fibers or optrodes, and viral injection sites. Mice were transcardially perfused under deep anesthesia with 50 mL of phosphate-buffered saline (PBS) followed by 50 mL of 4% w/v paraformaldehyde (PFA). Brains were postfixed overnight in 4% PFA and then dehydrated in 30% sucrose (in PBS) for at least 1 day. $50 \, \mu m$ coronal brain slices were serially cut with a sliding microtome using a cryostat (Leica Microsystems). The slices were counterstained with DAPI or Hoechst before imaging with an Olympus VS120 or VS200 virtual slide scanning microscope.

To confirm the expression of NaChBac, Kir2.1, and EGFP in PV-INs, immunostaining was performed on dmPFC sections (40 μm coronal brain slices) of NaChBac, Kir2.1 or EGFP expressing animals. Rabbit anti-PV was used as the primary antibody (PV 27, Swant; 1:2000), while Alexa Fluor 546 goat anti-rabbit IgG was used as the secondary antibody (1:1000, Thermo Fisher Scientific). The slices were then counterstained with DAPI before imaging with an Olympus VS120 or VS200 virtual microscopy slide scanning system.

QUANTIFICATION AND STATISTICAL ANALYSIS

All data are presented as mean ± SEM unless otherwise noted. Statistical analyses were performed using Prism 8.0 (GraphPad Software) or MATLAB 2021a (MathWorks). All statistical tests were two-tailed, and results were considered statistically significant when the *p* values were less than 0.05. Normality and equal variances between groups were assessed using the D'Agostino and Pearson omnibus normality test and Brown-Forsythe test, respectively. When normality and equal variance between sample groups were achieved, the paired t-test, unpaired t-test or Two-way repeated measure ANOVA with multiple comparisons was used. When normality or homogeneity of variance was not met, Wilcoxon Signed Rank Test, Wilcoxon matched-pairs signed rank test, Mann Whitney test or Friedman test with multiple comparisons test was performed. The Z test was used to assess the significance of the difference between two proportions, while the binomial test was used to evaluate whether the observed event probability matched the expected value. Pearson's correlation analysis was performed when normality of samples was achieved. More details are provided in the Table S1.